Doctoral Thesis

Analysis and Computer-Aided Simulation of Dressing of Grinding Wheel by Rotary Diamond Dresser

Mohammad Ashraful Karim Chowdhury

March 2014

Contents

Pages 4-6, 34, 56, 84, 89-90, 95-96, 100 are intentionally left blank.

Abstract

Grinding is often followed by dressing and vice versa. The objective of dressing is to sharpen the abrasive grains embedded on the working surface of a grinding wheel so that the wheel can keep its material removal efficiency. To achieve the objective, a dresser is needed and the dresser should operate in such a way so that it covers the whole working surface of the grinding wheel without covering the same area twice. Therefore, it is important to know the conditions that ensure this operating principle. This thesis deals with this issue in details. In particular, both analytical model of dressing and computer-aided simulation system are developed for determining the dressing performances for various conditions. The model is valid for a specific type of dresser called rotary diamond dresser. The thesis is structured, as follows:

Chapter 1 provides general overview of dressing and rotary diamond dresser. It also recalls the works related to development and simulation of different dressing method. Furthermore, performance of dressing is defined. Finally, the thesis organization is discussed in this chapter.

Chapter 2 deals with an analytical model of rotary diamond dresser while dressing a grinding wheel. The model establishes the relationships among the parameters that influence the surface topography of a grinding wheel, as well as the dressing performance. First, the geometric and kinematic parameters based on a model of the interaction between the grinding wheel and rotary diamond dresser is described. Based on this model, the length and sectional profile of dressing trajectory is defined.

The general properties of the dressing trajectory (length and sectional profile) are also described for a range of dressing conditions. From the general observations, it is found that the length of dressing trajectory is larger in case of Up-cut dressing than that of Down-cut dressing.

Chapter 3 describes a computer-aided simulation system to visualize the surface topography and the dressing performance of a grinding wheel after single/multiple passes. First, the requirements of the system are identified and described. The requirements are: Setting the surfaces for simulation and calculation, Determining the geometry of dressing trajectory, Determining the offset, Determining the coordinates of the starting point of a pass, Digitizing the effect of each dressing trajectory, Determining the dressing ratio, and Displaying the necessary inputs and outputs by both textural and graphical means. A system layout is also described to materialize the system. Afterward, the system developed is described showing the user-interface and system outputs (trajectory and dressing performance) for two different sets of dressing conditions.

Chapter 4 describes some useful results of dressing performance that has been found by using the system described in Chapter 3 for the case of 2D (i.e., considering the effect of dressing trajectory length, only). First, the dressing patterns are described for various conditions. This is followed by the study of determining the effect of the feed rate in single-pass dressing on the dressing performance. It is observed that complete dressing is almost impossible to achieve by tuning the feed rate of dresser in Down-cut dressing. In addition, the effect of number of passes in dressing is also described. It is found that lesser number of passes is required to realize complete dressing in Up-cut compared to Down-cut in multipass dressing. Finally, the

relationship between the number of passes and depth of cut for achieving the condition called complete dressing is also established.

Chapter 5 describes some results of 3D dressing performance (i.e., dressing performance based on the sectional profile of dressing trajectory). First, a model is introduced to represent the (real) surface profile of a grinding wheel. A model of simulating the resultant sectional profile (sectional profile of dressing trajectory for multiple passes of the dresser with the incremental depth of cut) is also described. Afterward, the interaction between the resultant sectional profile and real surface profile of grinding wheel is described. Finally, the 3D dressing performance is determined by computing the interaction between the resultant sectional profile and real surface profile of grinding wheel. It is evident after comparison that the value of dressing ratio is smaller for 3D performance analysis than that of 2D.

Chapter 6 provides the discussion and concluding remarks of the research study.

Chapter 1
Introduction

Grinding is one of the most important material removal processes for manufacturing precision parts. When the material removal efficiency of a grinding wheel decreases, the grinding wheel requires dressing [1,2]. Therefore, a grinding operation is often followed by a dressing operation and vice versa. The objective of a dressing operation is to sharpen the abrasive cutting edges embedded on the working surface of the grinding wheel [3]. In addition, dressing removes the bonds surrounding the abrasive grits and cleans out the layer of abrasive that is loaded on the grinding wheel. This way the material removal efficiency of a grinding wheel is restored.

There are many types of grinding wheel that are constructed with different kinds of abrasive grains, different grain spacing and different bond types. These abrasive grains are tiny, irregular shaped, and randomly oriented and positioned [4]. The abrasive grain is chosen depending on the hardness of the material being cut. Some commonly used abrasive grains are Aluminum Oxide, Silicon Carbide, Ceramic, Diamond and Cubic Boron Nitride. The conventional grinding wheels use Aluminum Oxide, Silicon Carbide or ceramic as abrasive grains. However, the grinding wheels that use Diamond or Cubic Boron Nitrid (CBN) are called superabrasive grinding wheel. The abrasive grains are hold in the bonding matrix which can be vitrified type, metal type, resin type etc. Bond types are chosen by

grinding method, truing method and workpiece materials [5]. Vitrified bond grinding wheels are extensively used mainly for precision and high efficiency grinding. Resin bond grinding wheels are used for rough grinding to finish grinding. However, metal bond is the strong bond compared with vitrified bond and resin bond, and metal bond grinding wheels are suitable for realizing high removal rate with accuracy and precision grinding of hard and brittle materials. After a grinding operation the abrasive grits on the circumferential surface of the grinding wheel become dull which decreases the grinding efficiency.

(a) Single Point Dresser

(b) Rotary Diamond Dresser

Figure 1.1. Different mechanical dressers.

As mentioned earlier, a dressing operation needs to be performed to restore the material removal efficiency of a grinding wheel. The dressing process determines the material removal rate, the grinding forces and the surface quality of the grinding

wheel [6]. It is worth mentioning that there are different types of dressing process: 1) Mechanical dressing with bonded abrasive tools, such as, single-point diamond dresser, Rotary Diamond Dresser (RDD) [3], etc. Mechanical dressing processes are the most common dressing processes and mechanical dressers (refer to Fig. 1.1) have one or multiple cutting edges or grits which can be distributed randomly or at regular intervals on the working surface of dressers. 2) Beam based dressing, e.g., abrasive water jet dressing [7] and laser beam dressing [8,9]. Beam based dressing is free of wear and can be used for any kind of grinding wheels. The important parameter of these types of dressing is the incoming beam in relation to the normal on grinding wheel [3]. 3) Electro-chemical/physical dressing, e.g., electro contact discharge dressing [10]. Electro contact discharge dressing is usually used in metal bonded grinding wheels due to electrical conductivity and the dressing is greatly dominated by discharge medium [11]. 4) Hybrid dressing [3]. These are not conventional dressing processes and are developed for specific purposes.

Among these different types of dressing, mechanical dressing is the most widely used and the rotary diamond dresser (RDD) is one of the most useful dressers, especially for the dressing of vitrified superabrasive grinding wheels, owing to its high wear resistance.

1.1 Rotary Diamond Dressing

Rotary diamond dressers have multiple cutting edges, i.e., diamond grits. While performing a rotary dressing operation (refer to Fig. 1.2), an overlap (called depth of cut) between the grinding wheel and dresser is created. At the same time, a relative motion is also maintained between the dresser and grinding wheel, which leads to an important parameter of rotary dressing process, the velocity ratio of

rotary diamond dresser to grinding wheel.

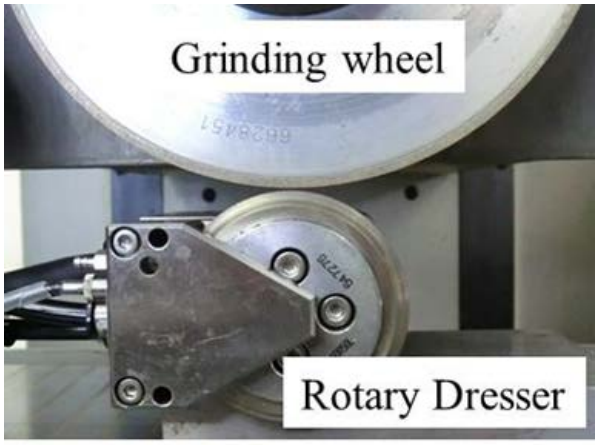

Figure 1.2. RDD set on a surface-grinding machine.

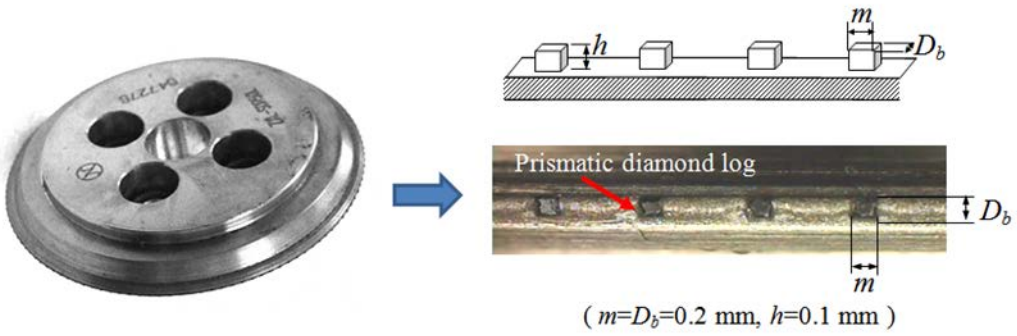

Figure 1.3. Prismatic monocrystalline RDD.

The functionality of the RDD depends on the number, shape and arrangement of diamond grits on its surface. In this study, we focus on a prismatic monocrystalline RDD. Figure 1.3 shows a photograph and optical image of a prismatic monocrystalline RDD, wherein equally sized monocrystalline diamond logs cut in a given crystal orientation are embedded onto the circumferential surface of the rotary dresser at regular intervals with a constant protrusion height h. The cross section of the diamond grits has the form of a square of a side $m = D_b$. This type of RDD is subjected to less wear and, thereby, has been widely used in the

dressing of grinding wheels for precision grinding. Using this type of RDD, we can carefully examine the dressing mechanism and the dressing performance, from which the geometrical uncertainty of the RDD is eliminated.

Rotary diamond dressers as a whole have better wear resistance capacity compared to fixed dressing tools as the dressing process is carried out by multiple cutting edges, i.e., grits. The RDD generates dressing trajectories on the working surface of the grinding wheel depending on the dressing strategies and dressing conditions. However, rotary diamond dressing creates highly complex dressing patterns on the grinding wheel surface. A systematic approach is required to understand this phenomenon. In this study, a model is developed for rotary diamond dressing based on kinematic analysis. Afterwards, a simulation based research is developed for the visualization of grinding wheel surface topography after rotary diamond dressing. This method and visualization enhances the overall efficiency and effectiveness of dressing and grinding as well.

1.2 Development and Simulation of Dressing Method

The grinding wheel surface topography resulting from dressing affects the performance of the subsequent grinding; therefore, the evolution of grinding wheel surface during dressing is an important research topic, and many authors have studied this issue from different perspectives. Focusing on the dressing methods, Kubo and Tamaki [12] developed a solid-type RDD consisting of a chemical vapor deposition (CVD) diamond disc and demonstrated that such an RDD results in a lower grinding force and a larger surface roughness than those of conventional RDDs. Tawakoli and Daneshi [13] developed a specially designed electroplated RDD called a T-dresser, which markedly reduces the grinding force and results in

almost the same ground surface roughness as that produced by a grinding wheel dressed with a conventional electroplated RDD. Mochida et al. [14] developed a single-point diamond dresser with a specific back rake angle and found that the back rake angle strongly affects the grinding wheel surface topography and the grinding performance. Focusing on the performance of rotary dressers, Huang [15] considered the resultant force acting on an individual grit of a vitrified diamond grinding wheel to evaluate the dressing efficiency of two types of rotary dresser: a SiC roll and a steel roll. Yamauchi et al. [16] investigated the dressing performance of two types of RDD, a metal-bonded RDD and a prismatic monocrystalline RDD [17] by conducting the internal grinding of a small bore. Mochida et al. [18] examined the performance of two types of dresser, a single-point diamond dresser and an RDD, in terms of the relationship between dressing force and grinding performance. Kim and Ahn [19] developed a sensor based systematic dressing strategy which suggests a proper dressing interval and an optimal dressing depth using the measurement data of the grinding wheel surface. Linke and Klocke investigated that bonding and abrasives of vitrified grinding wheel were molten during the dressing process by a diamond tile and form roller, which demonstrate the influence of dressing temperature on dressing performance [20].

The mechanical dressing of a vitrified grinding wheel can be considered as a type of cutting process in which a composite of abrasive grits and vitrified bonds is cut by a diamond tool and the transferability of the cutting path markedly affects the topography of the working surface of the grinding wheel. Especially, The RDD creates highly complex patterns on the working surface of the grinding wheel. Therefore, it is important to simulate the grinding wheel topography after dressing. Simulation assists decision making when optimizing the dressing and also when

designing new dressers. Doman et al. [21] reviewed the grinding wheel topography models that have been developed over half a century starting from the 1950s and proposed the important components and framework for a 3D topography model of a grinding wheel surface. Horng [22] presented a model to simulate the surface roughness in pad dressing using contact mechanics. This model considers the elastic-plastic deformation effects during grinding wheel wear. Klocke and Linke [23] developed a finite element model of a grinding wheel surface dressed with a single-point dresser and showed how the wheel wear is affected by the dressing parameters. Baseri et al. [24] developed a 2D topography model of a grinding wheel surface dressed with a rotary dresser that was based on a stochastic approach. This model can predict the number and angle of abrasive cutting edges generated on the grinding wheel surface. Bzymek et al. [25] developed a 3D topography model in which the effect of vibration generated from the RDD driving apparatus is considered. Moritomo et al. [26] introduced a stochastic model of an RDD on whose surface the diamond grits are placed at random, and derived the dressing ratio, i.e., the ratio of the dressed area to the whole surface of the grinding wheel. Yokogawa and Furukawa [27,28,29] developed a 3D topography model of a grinding wheel surface dressed with an RDD on whose surface the diamond grits are arranged at regular intervals. In this study, a simulation based research is conducted in the development of comprehensive dressing mechanism which is used to determine dressing performance. Furthermore, a computer-aided simulation is developed to visualize the two-dimensional [30,31,32,33] and three-dimensional [34,35] topography of a grinding wheel surface dressed by rotary diamond dresser. The developed simulation is an effective tool to foretell the dressing performance for chosen dressing conditions and strategies.

1.3 Performance of Dressing

The main objective of dressing is to sharpen the abrasive particles embedded on the working surface of a grinding wheel. To achieve this, the dresser grits should come in contact with the entire circumferential surface of a grinding wheel, known as complete dressing D_c, without hitting the same location repeatedly. In traverse dressing using an RDD, the dressing of the entire working surface of the grinding wheel, i.e., complete dressing, can be realized by single-pass dressing with a reasonably low traverse speed or by multipass dressing, in which depth of cut is given for each pass. Multipass dressing is also desirable for dressing by using a very small depth of cut (t around 2μm) so as to minimize the dressing force, and, thereby, the deformation. This way, one can achieve ultra-precision dressing and, as well as, grinding. One of the drawbacks of single-pass dressing is that the same area could be dressed several times. This is undesirable situation because the already-dressed abrasive particles might get dull or lose their sharpness again owing to abrasion with dresser. There is another issue, e.g., time required for completing the dressing either for single-pass or multipass dressing. The dressing time should be minimized to keep the economy of dressing and as well as grinding.

There have been no systematic studies that deal with the above-mentioned performance issues of dressing. In this study, these issues are addressed in a systematic manner from the perspective of a RDD. For the sake of better understanding, the study deals with the dressing mechanism on the basis of kinematic analysis at first and then deals with the evaluation of dressing performance by computer-aided simulation,

1.4 Thesis Structure

The remainder of this thesis is organized as follows:

Chapter 2 deals with an analytical model of rotary diamond dresser while dressing a grinding wheel. The model establishes the relationships among the parameters that influence the surface topography of a grinding wheel, as well as the dressing performance. First, the geometric and kinematic parameters based on a model of the interaction between the grinding wheel and rotary diamond dresser is described. Based on this model, the length and sectional profile of dressing trajectory is defined. The general properties of the dressing trajectory (length and sectional profile) are also described for a range of dressing conditions.

Chapter 3 describes a computer-aided simulation system to visualize the surface topography and the dressing performance of a grinding wheel after single/multiple passes. First, the requirements of the system are identified and described. A system layout is also described to materialize the system. Afterward, the system developed is described showing the user-interface and system outputs (trajectory and dressing performance) for two different sets of dressing conditions.

Chapter 4 describes some useful results of dressing performance that has been found by using the system described in Chapter 3 for the case of 2D (i.e., considering the effect of dressing trajectory length, only). First, the dressing patterns are described for various conditions. This is followed by the study of determining the effect of the feed rate in single-pass dressing on the dressing performance. In addition, the effect of number of passes in dressing is also described. Finally, the relationship between the number of passes and depth of cut for achieve the condition called complete dressing is also established.

Chapter 5 describes some results of 3D dressing performance (i.e., dressing

performance based on the sectional profile of dressing trajectory). First, a model is introduced to represent the (real) surface profile of a grinding wheel. A model of simulating the resultant sectional profile (sectional profile of dressing trajectory for multiple passes of the dresser with the incremental depth of cut) is also described. Afterward, the interaction between the resultant sectional profile and real surface profile of grinding wheel is described. Finally, the 3D dressing performance is determined by computing the interaction between the resultant sectional profile and real surface profile of grinding wheel.

Chapter 6 provides the discussion and concluding remarks of the research study.

Chapter 2
Analytical Model

This chapter deals with the analytical model of rotary diamond dresser while dressing a grinding wheel. That is to establish the relationships among the parameters that influence the surface topography of a grinding wheel [30,31,32]. For the sake of better understanding this chapter is organized in four sections, as follows: Section 2.1 describes the geometric and kinematic parameters based on a model of the interaction between the grinding wheel and rotary diamond dresser. Section 2.2 describes an analytical model of the length of dressing trajectory. Section 2.3 describes an analytical model of the sectional profile of dressing trajectory. Section 2.4 describes the general properties of the dressing trajectory (length and sectional profile).

2.1. Description of the Proposed Model

This section describes the geometric and kinematic parameters based on a model of the interaction between the grinding wheel and rotary diamond dresser.

Figure 2.1 schematically illustrates the sectional view of the proposed model of the interaction between the grinding wheel and rotary diamond dresser. As seen from Fig. 2.1, a grinding wheel of diameter D_g (radius r_g) rotates at a peripheral speed of V_g

centering a point denoted as O_g whereas the RDD of diameter D_d (radius r_d) rotates at a peripheral speed of V_d centering a point O_d. Due to this integration, two scenarios (hereinafter referred to as dressing strategy) arises. The first one is called *Down-cut* wherein the rotational directions of the grinding wheel and RDD are the same (see Fig. 2.1(a)). The other is called *Up-cut* wherein the rotational directions of the grinding wheel and RDD are the opposite (see Fig. 2.1(b)). In both cases, the depth of cut is given by *t*. A number of diamond grits, each having a length *m*, are uniformly embedded on the circumferential surface of the RDD. Figure 2.1 just depicts one of the diamond grits. Since all diamond grits have the same interaction, the analytical model based the grit shown in Fig. 2.1 is valid for all other grits, as well. The section view illustrated in Fig. 2.1 will be used to determine the length and sectional profile of the trajectory of a grit while performing dressing.

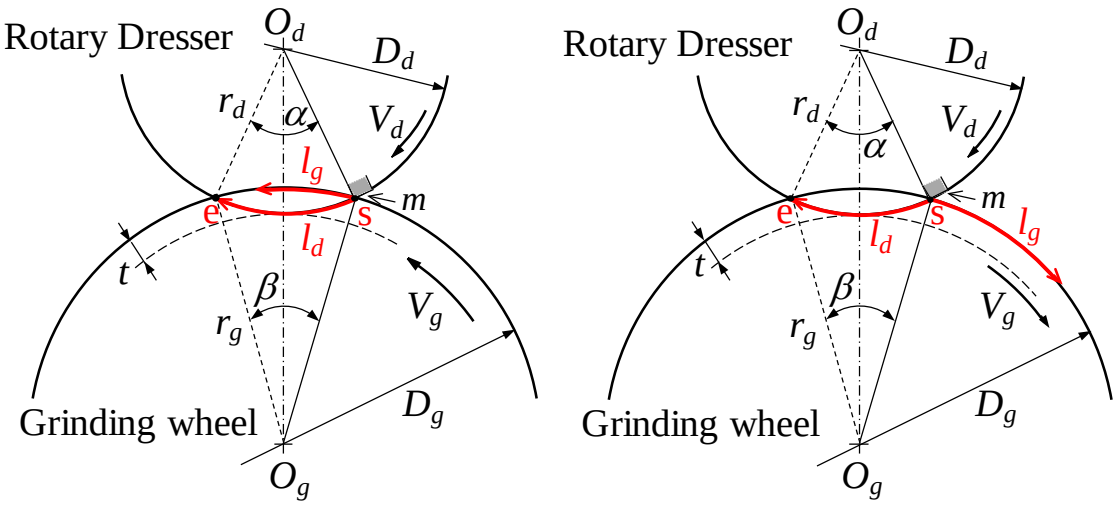

(a) down-cut (b) up-cut

Figure 2.1. The proposed model (sectional view).

Figure 2.2 schematically illustrates the outermost circumferential surface of the grinding wheel (i.e., birds-eye view) when two consecutive passes are applied in the opposite directions, which is adopted in this study. As seen from Fig. 2.2, there are some dressing trajectories (dressed area) oriented in accordance with the lead of the dresser.

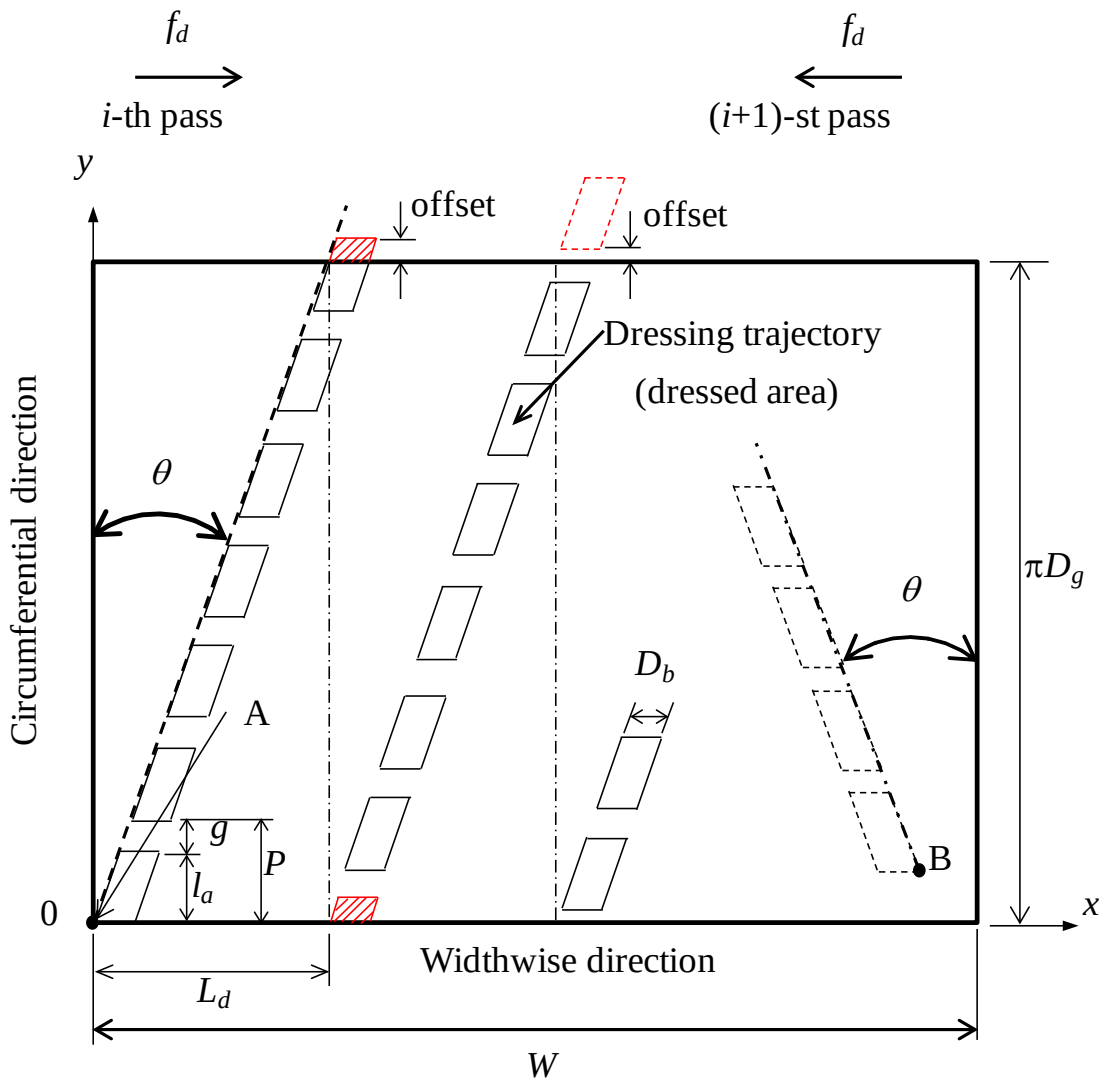

Figure 2.2. The proposed model (birds-eye view).

The representation of the model illustrated in Fig. 2.2 is helpful for visualizing the grinding wheel topography after some passes of dressing. As seen from Fig. 2.2, for the sake of visualization, a plane called x-y plane is considered, wherein x-axis is

parallel to the feed direction of the dresser and y-axis is parallel to the circumferential direction of the grinding wheel. As seen from Fig. 2.2, each diamond grit of the dresser creates a dressing trajectory on the outer circumferential surface of the grinding wheel. The x-axis corresponds to the width direction of the grinding wheel and the lines at $x = 0$ and $x = W$ are the side edges of the grinding wheel. The y-axis corresponds to the circumferential direction of the grinding wheel and the lines at $y = 0$ and $y = \pi D_g$ are the same lines on the circumferential surface of the grinding wheel. The RDD moves parallel to the x-axis in the left or right direction at a feed speed of f_d and forms a series of dressing trajectories with a dressing lead L_d.

The arrangement of the dressing trajectories, i.e., the dressing pattern formed on the circumferential surface of the grinding wheel, is determined by the pitch of two consecutive dressing trajectories P, the dressing lead L_d and the start points of a series of dressing trajectories, A and B, which are arbitrarily given at each dressing pass. The starting of dressing trajectories for the two consecutive passes may not be from the same location (compare the relative positions of points A and B in Fig. 2.2) because there is no guarantee that the dresser starts its operation from the same location every after each pass. The variability in the difference between the y-coordinates of A and B is randomly set in the range of P. Similarly, the difference between the x-coordinates of A and B may vary from pass to pass. This variability is randomly set in the range of L_d.

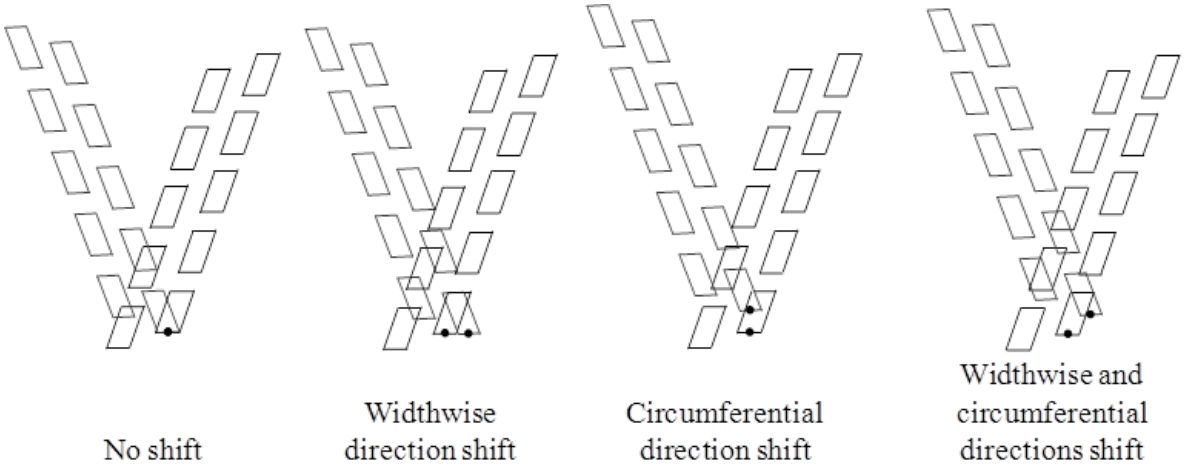

Figure 2.3. Possible orientations of the dressing trajectories in multiple passes.

As mentioned before, multiple passes are used to complete the dressing. A left-to-right pass is followed by a right-to-left pass and vice versa. As such, four situations as illustrated in Fig. 2.3 might occur: 1) the dressing trajectories are in phase, 2) the dressing trajectories are shifted in the widthwise direction only, 3) the dressing trajectories are shifted circumferential direction phase only, and 4) the dressing trajectories are shifted in both directions. The situation 1) is less likely to occur compared to the other situation as the dresser undergoes a time lag between two consecutive passes.

However, a set of parameters are needed to define the model presented in Figs. 2.1-3. These parameters are listed in Table 2.1. The meaning of each parameter, along with the notation, is also listed in Table 2.1.

Table 2.1. Parameters underlying the proposed model of dressing.

Symbol	Meaning
D_g (r_g)	Diameter (radius) of grinding wheel
W	Width of grinding wheel
V_g	Peripheral speed of grinding wheel
N_g	Rotational speed of grinding wheel
D_d (r_d)	Diameter (radius) of rotary diamond dresser
V_d	Peripheral speed of rotary diamond dresser
α, β	Included angle of RDD, grinding wheel, respectively
n	Number of diamond grits on rotary diamond dresser
m	Length of diamond grits on rotary diamond dresser
D_b	Width of diamond grits on rotary diamond dresser
t	Depth of cut in dressing
t_c	Critical depth of cut in dressing
VR	Velocity ratio of rotary diamond dresser to grinding wheel (V_d / V_g)
f_d	Feed speed of rotary diamond dresser
L_d	Dressing lead (f_d / N_g)
θ	Lead angle of dressing
FR	Feed rate of rotary diamond dresser (L_d / D_b)
N_D	Number of passes in dressing
l_a	Length of dressing trajectory
P	Pitch of dressing trajectory
g	Gap between two consecutive dressing trajectories
D_r	Dressing ratio
+, -	Up-cut (+VR), Down-cut (-VR)

2.2. Length of Dressing Trajectory

This section describes how to determine the length of dressing trajectory (l_a). To do this, a derived parameter called equivalent diameter denoted as (D_{eg}) is needed. Therefore, in the remainder of this section first D_{eg} is defined and based on that l_a is defined afterward.

Recall Fig. 2.1. The front end of diamond grit first comes in contact with the grinding wheel at point *s* and terminates its contact at point *e*.

The length l_d measured from the point *s* to point *e* along the circumference of the RDD is given as

$$l_d = 2\sqrt{D_{eg}t}\,. \tag{2.1}$$

In equation (2.1) D_{eg} is the equivalent diameter and given as

$$D_{eg} = \frac{D_g D_d}{D_g + D_d} \tag{2.2}$$

This yields the following expression of contact period T :

$$T = \frac{l_d}{V_d} = \frac{2\sqrt{D_{eg}t}}{V_d} \tag{2.3}$$

During the contact period, point s on the outermost surface of the grinding wheel moves by a distance l_g along the circumference of the grinding wheel to another point. l_g is given as

$$l_g = TV_g = 2\sqrt{D_{eg}t}\,\frac{V_g}{V_d} \tag{2.4}$$

When the depth of cut t is very small compared with D_g and D_d, the length l_d measured along the circumference of the RDD is almost equal to the length of the circular arc se measured along the circumference of the grinding wheel. Therefore, the length of the dressing trajectory of the front end of a diamond grit l'_a, which is measured along the circumference of the grinding wheel, is given as

$$l'_a = l_d \pm l_g = \left|\left(2\sqrt{D_{eg}t}\right) \pm \frac{V_g}{V_d}\left(2\sqrt{D_{eg}t}\right)\right| = \left|1 \pm \frac{V_g}{V_d}\right|\left(2\sqrt{D_{eg}t}\right) \tag{2.5}$$

In Eq. (2.5), the plus sign is applied in the case of up-cut dressing and the minus sign is applied in the case of down-cut dressing.

Since the length of the diamond grit is m, its rear end will come in contact with the grinding wheel after a period T_m given as

$$T_m = \frac{m}{V_d} \tag{2.6}$$

In time T_m, the grinding wheel also travels the circumferential distance

$$l_m = T_m V_g = \frac{V_g}{V_d} m \tag{2.7}$$

Thus, the length of the dressing trajectory of a diamond grit l_a, which is measured along the circumference of the grinding wheel, is given as

$$l_a = l'_a + l_m = 2\left|1 \pm \frac{V_g}{V_d}\right|\sqrt{D_{eg}t} + \frac{V_g}{V_d}m \tag{2.8}$$

The pitch of the dressing trajectories formed on the circumferential surface of the grinding wheel (see Fig. 2.2) is given as

$$P = \frac{V_g}{V_d} \cdot \frac{\pi D_d}{n} \tag{2.9}$$

Where n is the number of diamond grits on the surface of the RDD.

The gap between two successive trajectories l_a (see Fig. 2.2) is given as

$$g = P - l_a \tag{2.10}$$

If $g > 0$, a series of separated dressing trajectories is generated on the surface of the grinding wheel, as schematically shown in Fig. 2.2. If $g < 0$, the dressing trajectories overlap with each other, and a series of continuous trajectories is generated.

Every after each rotation of the grinding wheel, the dressing trajectories are repeated with an offset in the feed direction called lead L_d, which is the linear distance that the dresser travels in the direction of feed by one revolution of the grinding wheel. Thus,

$$L_d = \frac{f_d}{N_g} \tag{2.11}$$

The form and size of each dressing trajectory are determined by the length l_a, the width D_b and the angle of the dressing lead θ. The angle (θ) that the dressing trajectories make

with the circumferential direction is as follows:

$$\theta = tan^{-1}\sqrt{\frac{f_d}{N_g(\pi D_g)}} \tag{2.12}$$

Sometimes, a part of the dressing trajectory exceeds the circumferential length (πD_g), as shown by the hatched area in Fig. 2.2. In such cases, the area that exceeds the circumferential distance is placed in the starting of the next cycle, as it is seen from Fig. 2.2. This means that the dressing trajectories may or may not start from the same location of *x*-axis after each revolution of the grinding wheel. Therefore, the dressing trajectories may have a certain amount of offset when they are repeated for each rotation of the grinding wheel. There are two different cases of offset as shown in Fig. 2.2. Note that an offset part of the dressing trajectory of length l_a and an offset part of the undressed part given by a gap g, both of which are located on the exterior of the *x*-*y* plane, are folded back at $y = \pi D_g$ to move them to the position $y = 0$, at which the next series of dressing trajectories starts.

2.3. Sectional Profile of Dressing Trajectory

The sectional profile of dressing trajectory consists of trochoid curves and straight line. This section describes how the sectional profile of dressing trajectory is derived in the analytical model.

The relative positions of the dressing trajectories of the front end and rear end points of a diamond grit on the grinding wheel are illustrated in Fig. 2.4.

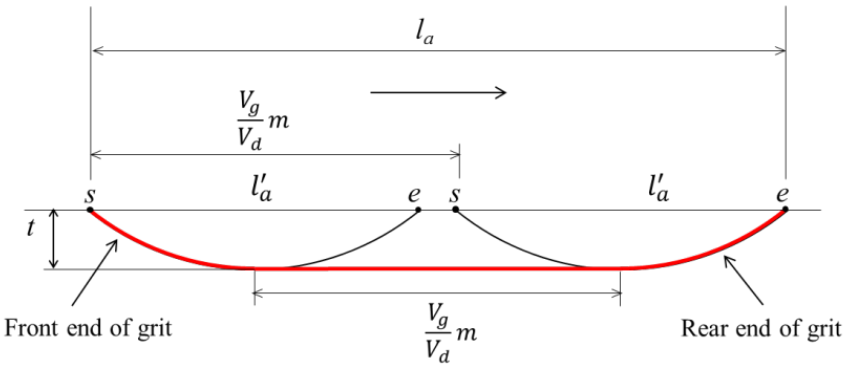

Figure 2.4. Sectional profile with respect to dressing trajectory.

As shown in Fig. 2.5, the sectional profile of the dressing trajectory is formed by two trochoid curves, curve AB at the front and curve CD at the rear, and the straight line segment BC connecting the two curves. When the depth of cut t is very small compared with D_g and D_d, the trochoid curve can be approximated by a parabola. Taking this into consideration, the sectional profile (l, z) of the dressing trajectory can be expressed as

$$\begin{cases} z = t - \dfrac{l^2}{D_{eg}\left(1 \pm \dfrac{V_g}{V_d}\right)^2} & -\dfrac{l_a}{2} \le l \le -\dfrac{1}{2}\dfrac{V_g}{V_d}m \\ z = t & -\dfrac{1}{2}\dfrac{V_g}{V_d}m < l \le \dfrac{1}{2}\dfrac{V_g}{V_d}m \\ z = t - \dfrac{l^2}{D_{eg}\left(1 \pm \dfrac{V_g}{V_d}\right)^2} & \dfrac{1}{2}\dfrac{V_g}{V_d}m < l \le \dfrac{l_a}{2} \end{cases} \tag{2.13}$$

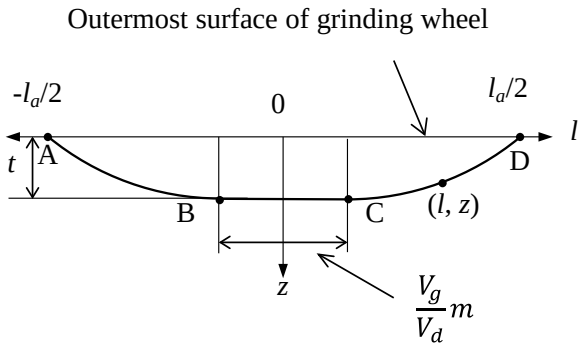

Figure 2.5. Mathematical representation of sectional profile.

2.4. General Properties of Dressing Trajectory

Table 2.2. Dressing conditions.

Grinding wheel diameter	D_g = 140 mm
Grinding wheel velocity	V_g = 36.7 m/s (5000 rpm)
Rotary dresser	Monocrystalline diamond roll
Diameter of dresser	D_d = 50 mm
Number of diamond grits	n = 120
Length of diamond grits	m = 0.2, 0.4, 1.0 mm
Width of diamond grits	D_b = 0.2 mm
Depth of cut in dressing	t = 2, 4, 6, 8 μm
Velocity ratio	$VR = V_d/V_g$ = 0～±2.0 (+:Up-cut, -:Down-cut)
Feed speed of dresser	f_d = 1～5000 mm/min
Dressing lead	L_d = 0. 2～1000 μm/rev
Feed rate of dresser	FR = 0.001～5.0
Number of times of dressing	N_D = 1～20

This section describes the general properties of dressing trajectory in terms of the length of dressing trajectory and sectional profile. A related concept called critical depth of cut (t_c) of dressing is also described. To understand the general properties a wide range values of the dressing parameters (Table 2.1) are needed. In this study the range of values listed in Table 2.2 are used.

2.4.1. Properties of Length of Dressing Trajectory

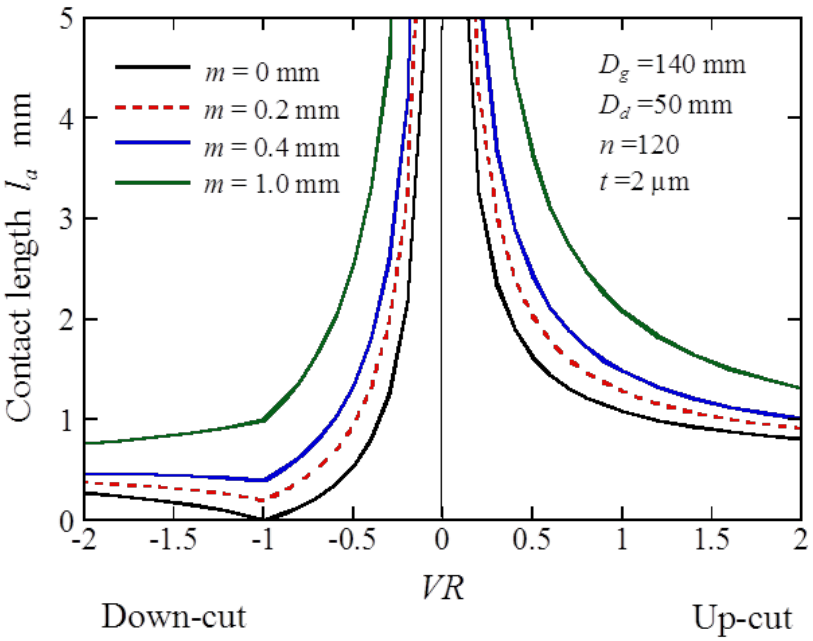

Figure 2.6. Relationship between l_a and VR (parameter m).

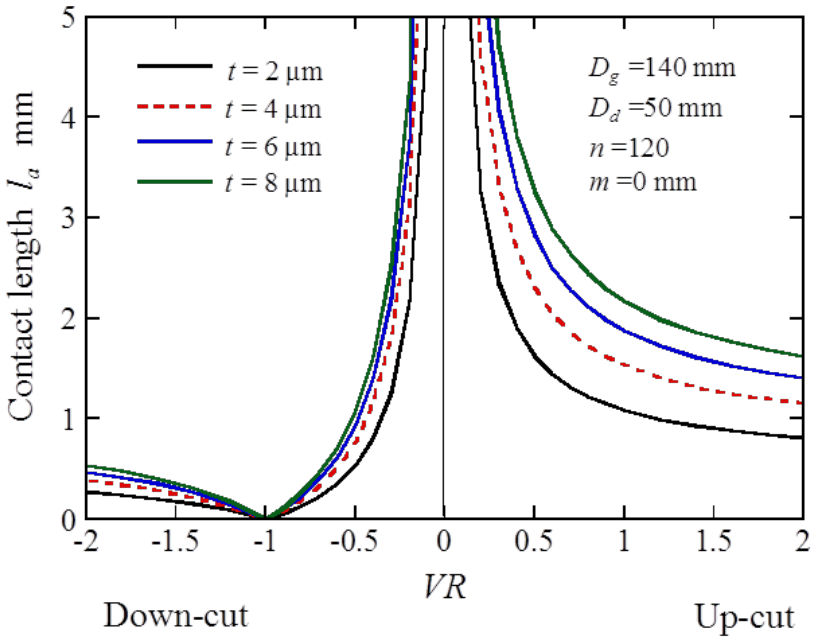

Figure 2.7. Relationship between l_a and *VR* (parameter *t*).

Figures 2.6 and 2.7 show the calculated curves of the contact length l_a for various values of *VR*, which is defined as the velocity ratio of the RDD to the grinding wheel ($VR = V_d / V_g$). In the figures, negative values of *VR* indicate down-cut dressing and positive values indicate up-cut dressing. The effect of the length of the diamond grit *m* is shown in Fig. 2.6 and that of the depth of cut *t* is shown in Fig. 2.7. It can be seen from the figures that l_a increases with *m* and *t*, respectively, for all values of *VR*. By examining the effect of *VR*, it can be seen that the value of l_a in the case of down-cut dressing is less than that in the case of up-cut dressing for a given absolute value of *VR*. It can also be seen that an inflection point exists at *VR* = -1 in down-cut dressing. This is due to the contact length between a diamond grit of the RDD and the grinding wheel decreasing as the value of *VR* approaches -1, becoming zero at *VR* = -1 and increasing away from the value of *VR* = -1. The dressing process at *VR* = -1 is called crush-mode dressing.

2.4.2. Properties of Sectional Profile of Dressing Trajectory

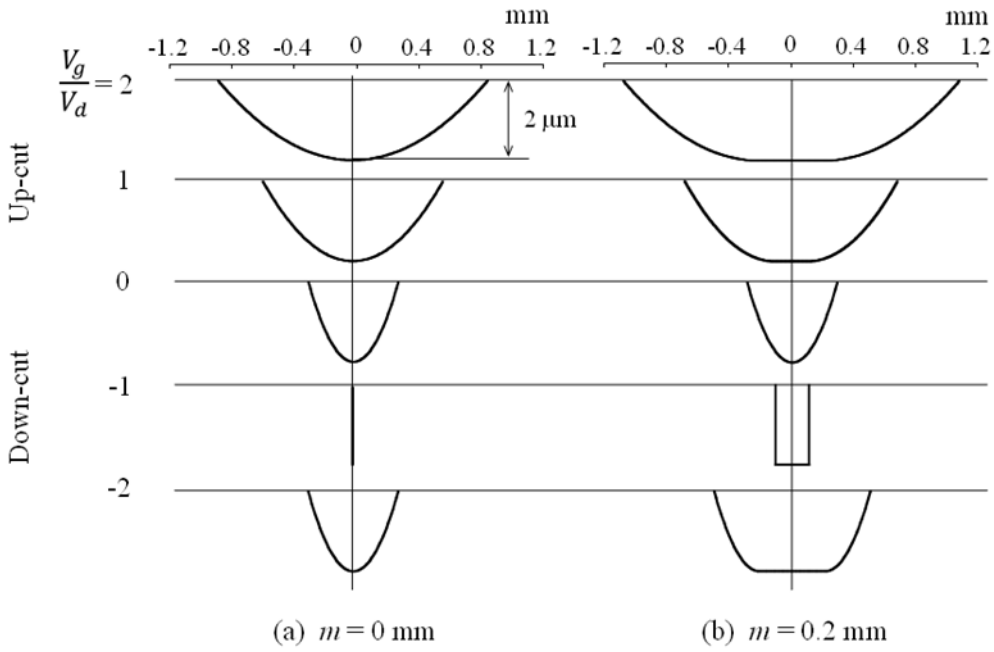

Figure 2.8. Sectional profiles of dressing trajectory (parameters, V_g/V_d and m).

Figure 2.8 shows the sectional profiles of dressing trajectories to illustrate the effects of the length of diamond grits m and the dressing strategy, i.e., up-cut dressing or down-cut dressing. These profiles were calculated by substituting the dressing conditions listed in Table 1 into Eq. (2.13). Note that the velocity ratio V_g/V_d shown in Fig. 2.8 is the inverse of VR shown in Figs. 2.6-2.7. $V_g/V_d = 0$ in Fig. 2.8 means that the grinding wheel stops rotating and only the RDD rotates; therefore, the sectional profile of the dressing trajectory is that of the grinding wheel surface, whose diameter is given by Eq. (2.2). In Fig. 2.8, V_g/V_d = -2, -1, 1 and 2 correspond to VR = -0.5, -1, 1 and 0.5 in Figs. 2.6-2.7, respectively.

2.4.3. Critical Depth of Cut in Dressing

The critical depth of cut in dressing t_c that realizes continuous dressing trajectories is derived by substituting l_a given by Eq. (2.8) and P given by Eq. (2.9) into Eq. (2.10) and setting g equal to zero as follows:

$$t_c = \left(\frac{1}{D_{eg}}\right)\left[\frac{\frac{V_g}{V_d}\left(\frac{\pi D_d}{n}-m\right)}{2\left|1\pm\frac{V_g}{V_d}\right|}\right]^2 \tag{2.14}$$

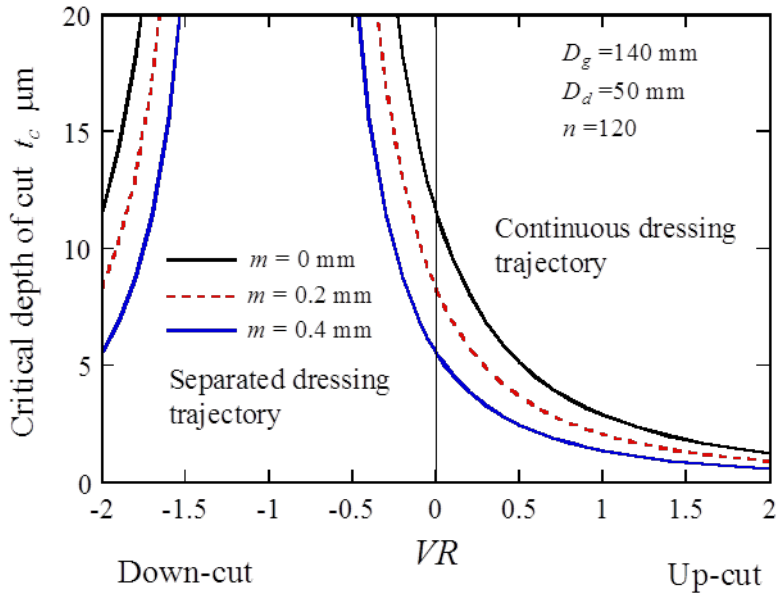

Figure 2.9. Relationship between t_c and VR (parameter m).

Figure 2.9 shows the calculated curves of t_c for various values of VR. The three curves are for m =0, 0.2 and 0.4 mm. It can be seen from the figure that the maximum t_c is 5 to 10 μm in the case of up-cut dressing; however, in the case of down-cut dressing, it exceeds 20 μm for almost all values of VR. From Fig. 2.9, the dressing conditions that

realize continuous dressing trajectories can be obtained. For example, in the case of m = 0.2 mm, t = 2 μm and up-cut dressing, it can be seen from the figure that continuous dressing trajectories are formed when VR is greater than 1.0.

Chapter 3
Computer-Aided Simulation System

This chapter deals with the computer-aided simulation system that has been developed to visualize the trajectories of the dresser on the circumferential surface of the grinding wheel so as to get some useful feedbacks on the dressing performance. For the sake of better understanding this chapter is organized in five sections, as follows: Section 3.1 describes the general requirements of the proposed simulation system. Section 3.2 describes the concept called dressing performance. Section 3.3 describes the parameters needed to perform the simulation. Section 3.4 describes the procedure to set a representative area for determining the dressing performance. Section 3.5 describes the system developed.

3.1. Requirements of the Proposed Simulation System

This section describes the general requirements of the proposed simulation system. To describe the general requirements, a schematic illustration as shown in Fig. 3.1 is introduced. This illustration is quite similar to that of Fig. 2.2. As seen from Fig. 3.1, to develop a computer-aided simulation system for visualizing the surface topography of the grinding wheel after dressing and determining the performance of

dressing, there are some requirements. These requirements are described as follows:

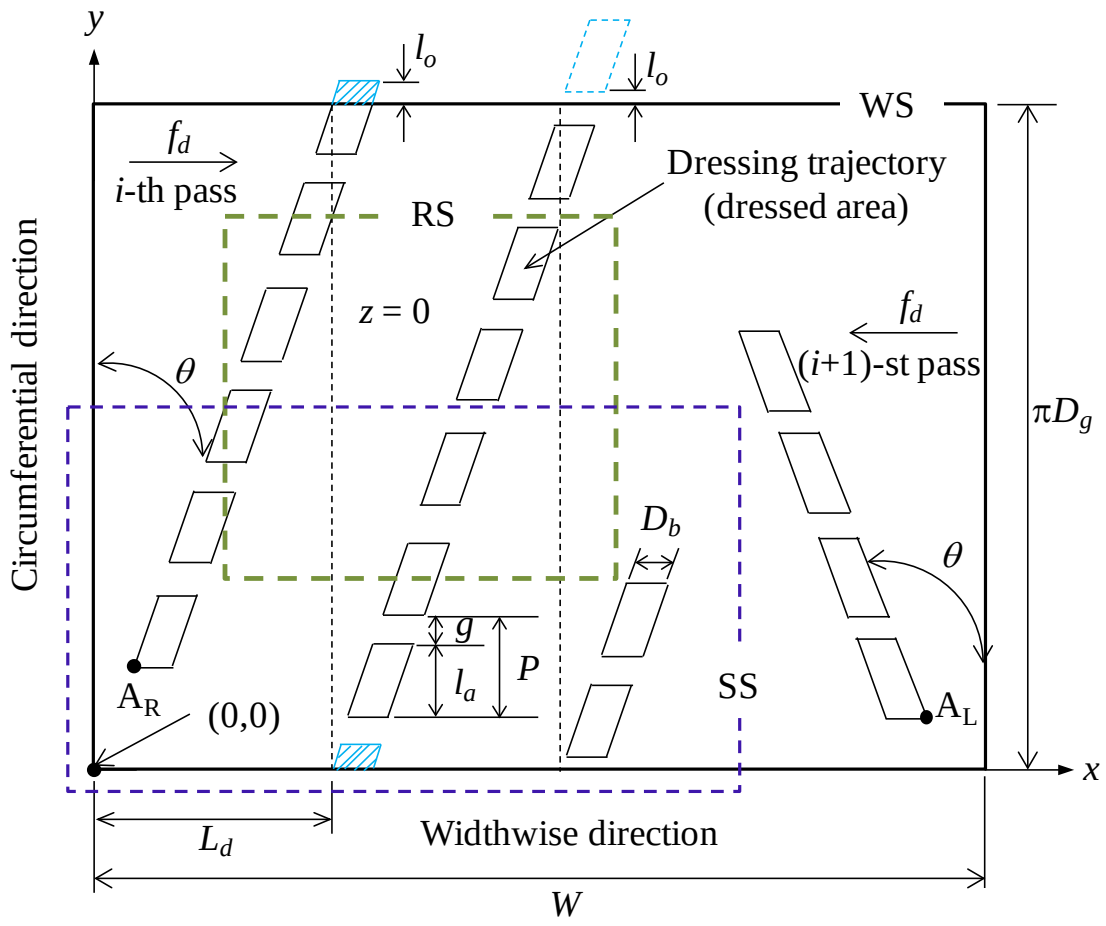

Figure 3.1. Schematic illustrations the requirements of the proposed computer-aided simulation system.

Requirement 1: Requirement 1 means setting the surfaces for simulation and calculation. In this case, three types of surfaces can be imagined. There are three types of surfaces. The first one is called working surface (WS). The second one is called simulation surface (SS). The other surface is called representative surface (RS). Figure 3.1 schematically illustrates these surfaces on a plane $z = 0$, which is the outer most plane on the circumferential surface of the grinding wheel. In this chapter, the attention will be given on the planes for $z = 0$. The planes for $z < 0$ (i.e., planes in the depth-wise

direction) will be considered in Chapter 5. The simulation is not performed for the whole WS as it is a relatively large area. Simulation is performed for the planes bounded by SS whereas the dressing performance (addressed below) is determined based on RS. As such, RS should be a surface inside the SS. The relative position of SS and RS is described in Fig. 3.2. The dressing trajectories are created in the SS.

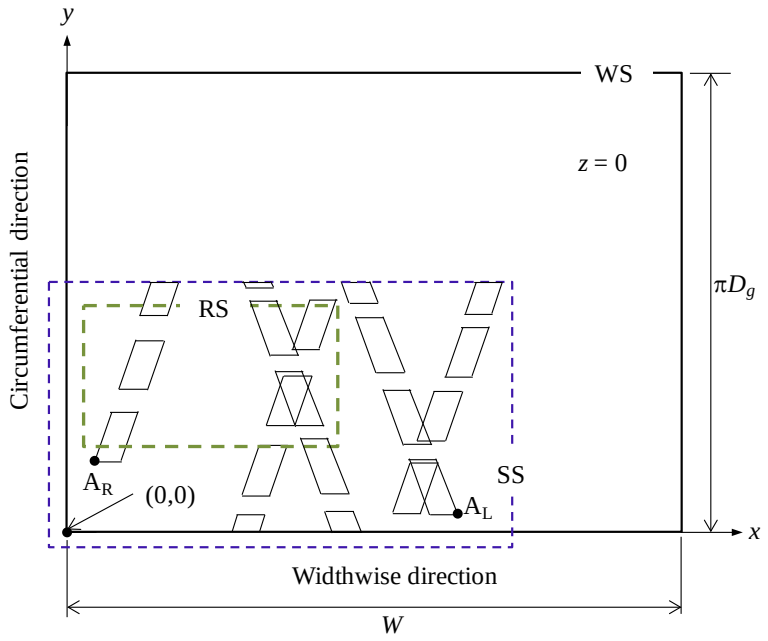

Figure 3.2. Relative positions of WS, SS and RS.

Requirement 2: Requirement 2 means determining the geometry of the dressing trajectory. The geometry of the dressing trajectory is schematically illustrated in Fig. 3.3. As seen from Fig. 3.3., a dressing trajectory is a parallelogram. The height of the parallelogram is l_a as defined in (2.8) and the width is D_b. The gap between two nonconsecutive trajectories is given by g as defined in (2.10). The gap (g) is controlled by using the pitch P (as defined in (2.9)) and l_a. The case shown in Fig. 3.3 corresponds to a positive gap, i.e., no overlapping of trajectories. Note that the gap could be negative. In this case, two nonconsecutive trajectories overlap. (See Chapter 4 for the examples.)

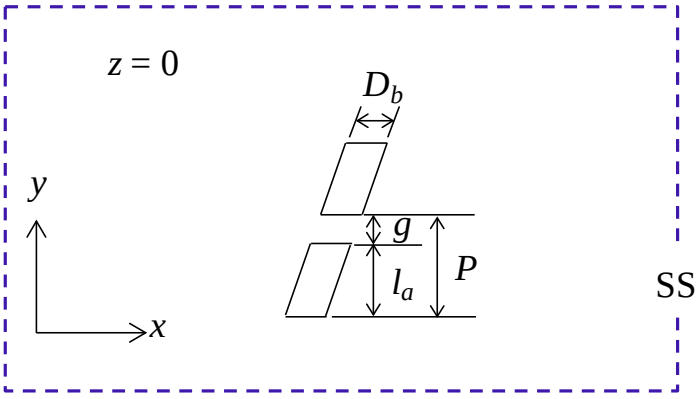

Figure 3.3. The geometry of a dressing trajectory.

According to the above description, to calculate the dimensions of a trajectory (l_a, D_b, P, g), a produce is needed. In dressing the usual practice is to input the values of the following parameters (hereinafter referred to as independent variables): Vg, $+VR$ (up cut), $-VR$ (down cut), D_g, D_d, D_b, N_D, m, n, f_d, and t (see Table 2.2). As described in Chapter 2, these parameters help determine three dependents variables, i.e., D_{eg}, L_d, V_d, N_g. Afterward, the dimensions of the dressing trajectory, i.e., l_a, D_b, P, and g, are determined from the independent and dependent variables. Note that the independent variable f_d and two dependent ones (L_d and N_g) are not used at this stage. They are used while determining the orientation of the trajectories.

Requirement 3: Requirement 3 means determining the orientation of the trajectories. Due to f_d and the type of pass (even or odd pass), the orientation of the trajectories change, as schematically illustrated in Figs. 3.1-2. The odd passes are the 1st pass, third pass, fifth pass, and so on whereas the even passes are the 2nd pass, 4th pass, and so on. As seen from Figs. 3.1-2, the odd passes are oriented toward the left-to-right direction whereas the even passes are oriented toward the right-to-left pass. Two consecutive passes act in the opposite directions. However, to set the orientation, one

needs to calculate L_d and θ. These parameters are defined in (2.11 and 2.12). Thus, a dressing trajectory (Fig. 3.2) is rotated around the *y*-axis at an angle θ in the clockwise direction, if it is an odd pass. On the other hand, a dressing trajectory (Fig. 3.1) is rotated around the *y*-axis at an angle θ in the anticlockwise direction, if it is an even pass.

Requirement 4: Requirement 4 means determining the offset (l_0). For the accurate representation of the dressing trajectories after each full rotation of the grinding wheel as schematically illustrated in Fig. 3.1, an offset should be incorporated. There are three possible scenarios regarding the offset, as illustrated in Fig. 3.4.

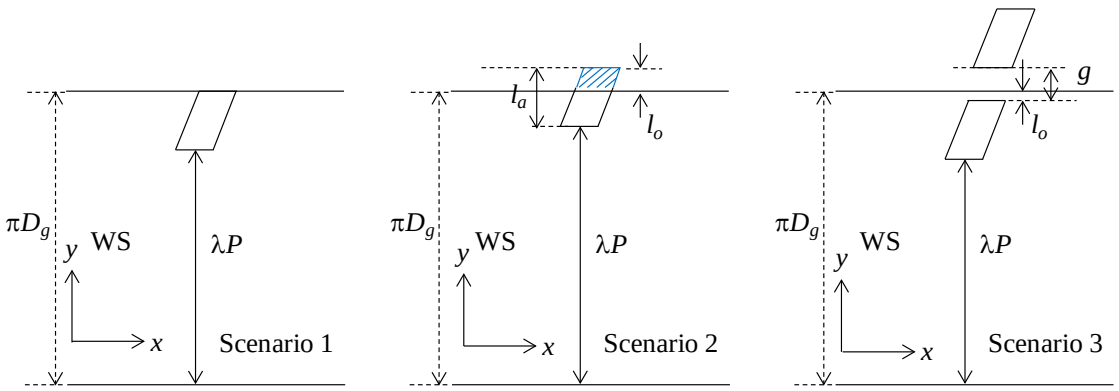

Figure 3.4. Possible scenarios of offset.

As seen from Fig. 3.4, the scenario 1 represents a *zero* (or no) *offset*, the scenario 2 represents a *trajectory-cut offset*, and the scenario 3 represents a *gap-cut offset*. To ensure the type of scenario an integer λ ($\in \aleph$) can be considered that fulfill the condition defined in equation (3.1).

$$\left(\lambda P < \pi D_g\right) \wedge \left((\lambda + 1)P > \pi D_g\right) \tag{3.1}$$

As such, the offset is calculated by using the following equation:

$$l_o = \begin{cases} 0, \ \lambda P + l_a = \pi D_g \\ (\lambda P + l_a) - \pi D_g, \ \lambda P + l_a > \pi D_g \\ \pi D_g - (\lambda P + l_a), \ otherwise \end{cases} \quad (3.2)$$

For l_o corresponding to scenario 2, the length of the last trajectory is equal to l_a-l_o and the length of the first trajectory in the next rotation is equal to l_o. For l_o corresponding to scenario 3, the first trajectory of the next rotation starts from a distance g-l_o in the y-axis direction.

Requirement 5: Requirement 5 means determining the coordinates of the starting point of a pass denoted as $A_R = (x_{AR},y_{AR})$ or $A_L = (x_{AL},y_{AL})$, as illustrated in Fig. 3.1. Figures 3.5-6 schematically illustrate the position of A_R and A_L, respectively.

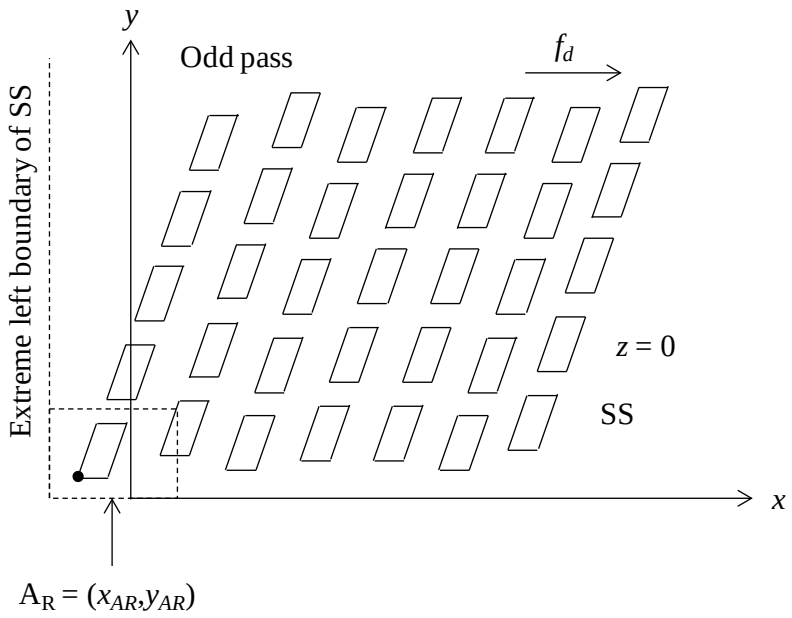

Figure 3.5. Starting point of an odd pass.

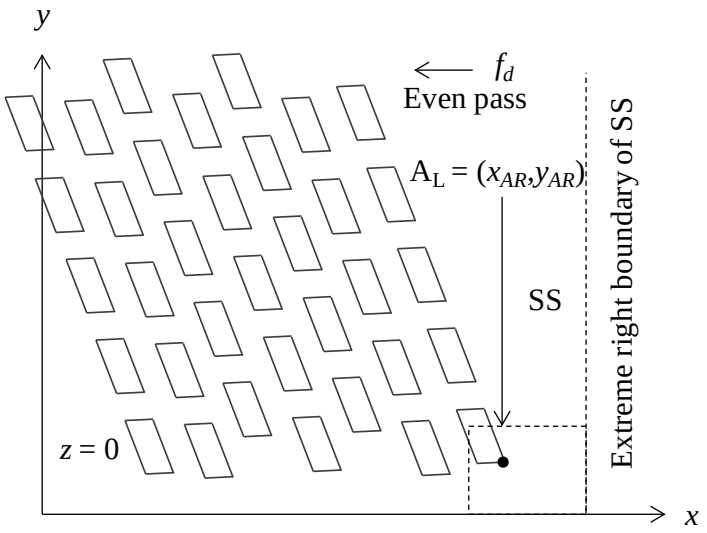

Figure 3.6. Starting point of an even pass.

The position of these points should randomly be created because there is no guarantee that the dresser starts its operation from the same location every after each pass. Therefore, the coordinates of these points should randomly be generated as defined in the following equations.

$$x_{AR} = x_{SSL} + r \cdot L_d \tag{3.3}$$

$$x_{AL} = x_{SSR} - r \cdot L_d \tag{3.4}$$

$$y_{A(R\ or\ L)} = r \cdot P \tag{3.5}$$

In equations (3.3)-(3.5), r denotes a random number in the interval [0,1], x_{SSL} denotes the x-coordinate of the leftmost boundary line of SS, and x_{SSR} denotes the y-coordinate of the rightmost boundary line of SS. However, by convention, the first pass starts at the origin (0,0), i.e., for the first pass $A_R = (x_{AR}, y_{AR}) = (0,0)$.

Requirement 6: Requirement 6 means digitizing the effect of each dressing trajectory belonging to the boundary of RS. One may set it (RS) as preferred inside the SS, as schematically illustrated in Fig. 3.2. Let RS(k,q), k = 1,2,...,K, q = 1,2,...,Q, be a cell of a 2D array representing the RS, wherein k denotes the k-th row and q denotes the q-th column. The conditions of SB(k,q) can be represented by $BD_{ij}(k,q)$ and $AD_{ij}(k,q)$. Here, "BD" means "before dressing" and "AD" means "after dressing." The index i represents the i-th pass and j represents the j-th trajectory of that pass. Here, J represents the number of trajectory created considered for RS, i.e., $j \in \{1,2,...,J\}$ and I represents the number of passes applied while performing the dressing operation, i.e., $i \in \{1,2,...,I\}$.

The digitization can be performed based on two assumptions. The first one is digitization based on perfect surface. The other one digitization is based on real surface. In the case of digitization based on perfect surface, $\forall BD_{ij}(k,q) = 0$ and $\forall AD_{ij}(k,q) \in \{0, 1\}$. This means that all cells in $BD_{ij}(k,q) = 0$ (a perfect plane surface) and are converted to $AD_{ij}(k,q)$ that is a digit equal to 1 or 0. The conversion is schematically illustrated in Fig. 3.7.

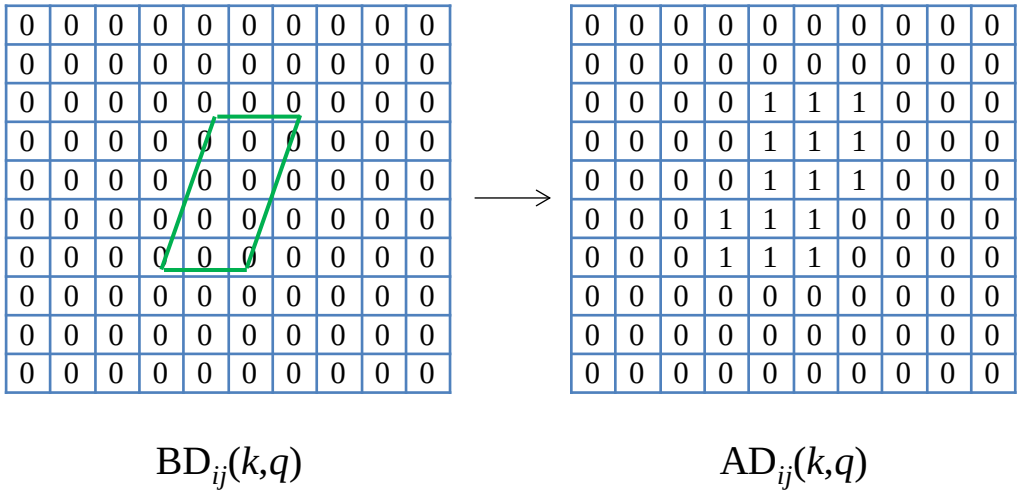

Figure 3.7. Digitization of RS based on perfect surface.

As seen from Fig. 3.7, the following rule is needed to create $AD_{ij}(k,q)$ from $BD_{ij}(k,q)$:

If the *j*-th trajectory of the *i*-th pass be on the cell $BD_{ij}(k,q)$ either partially or fully, *then* $AD_{ij}(k,q) = 1$, otherwise $AD_{ij}(k,q) = BD_{ij}(k,q) = 0$.

On the other hand, in the case of digitization based on real surface, $BD_{ij}(k,q)$ is not always zero. This means that some $BD_{ij}(k,q) = 0$ and some other $BD_{ij}(k,q) < 0$, i.e., $BD_{ij}(k,q) \leq 0$. The less the value of $BD_{ij}(k,q)$ is the deeper the surface of the grinding wheel is. Figure 3.8 schematically illustrates how $BD_{ij}(k,q)$ converts to $AD_{ij}(k,q)$. The cells which are not covered either partially or fully by the *j*-th trajectory of the *i*-th pass correspond to $AD_{ij}(k,q) = BD_{ij}(k,q)$. The other cells $AD_{ij}(k,q)$ (denoted as *zg*) are created after considering the sectional profile height of a trajectory (see equation (x.x)). Let $z_{ij}(k,q)$ be the magnitude (i.e., $z_{ij}(k,q)$ is a positive real number) of the depth of the sectional profile of the *j*-th trajectory of the *i*-th pass on the cell RS(*k*,*q*) of RS. This yields the following rule for creating $AD_{ij}(k,q)$ from $BD_{ij}(k,q)$:

If $-z_{ij}(k,q) \leq BD_{ij}(k,q)$ then $AD_{ij}(k,q)$ (= *zg*) = $-z_{ij}(k,q)$, otherwise, $AD_{ij}(k,q)$ (= *zg*) = $BD_{ij}(k,q)$.

-2	0	0	-2	0	0	-2	-0	-1	0
0	0	0	0	0	0	-1	-1	0	-1
-1	-2	0	-2	-4	0	0	-2	-1	0
-1	0	0	0	0	-2	0	0	-2	0
-4	0	-2	0	-5	-3	-1	0	-2	-2
-1	0	-4	0	-1	-1	-2	-2	0	0
-1	0	-3	0	0	-3	0	0	-2	0
-1	0	-1	0	0	0	0	0	0	0
0	0	-0	0	-1	-0	-1	0	0	-2
-2	-3	0	-2	0	-2	-3	-2	0	0

$BD_{ij}(k,q)$

-2	0	0	-2	0	0	-2	-0	-1	0
0	0	0	0	0	0	-1	-1	0	-1
-1	-2	0	-2	*zg*	*zg*	*zg*	-2	-1	0
-1	0	0	0	*zg*	*zg*	*zg*	0	-2	0
-4	0	-2	0	*zg*	*zg*	*zg*	0	-2	-2
-1	0	-4	*zg*	*zg*	*zg*	-2	-2	0	0
-1	0	-3	*zg*	*zg*	*zg*	0	0	-2	0
-1	0	-1	0	0	0	0	0	0	0
0	0	-0	0	-1	-0	-1	0	0	-2
-2	-3	0	-2	0	-2	-3	-2	0	0

$AD_{ij}(k,q)$

Figure 3.8. Digitization of RS based on real surface.

Requirement 7: Requirement 7 means determining the dressing ratio (D_r). It is a measure that quantifies the degree of dressing. If the RS is dressed fully then D_r is equal to 1 otherwise, $D_r \geq 0$. This means that D_r = [0,1]. The more the value of D_r is the more the dressed area is. The dressing ratio of a given pass (say i-th pass, denoted as D_{ri}) can be determined as follows:

$$D_{ri} = \frac{\sum_{j=1}^{J}\left(\sum_{k}^{K}\left(\sum_{q}^{Q} \mathrm{AD}_{ij}(k,q)\right)\right)}{K \cdot Q . J} \tag{3.6}$$

The dressing ratio of up to a given number of passes (i.e., i passes denoted as D_{r+i}) is the cumulative effects of 1-st, 2-nd, ..., i-th passes. This it is given as:

$$D_{r+i} = \frac{\sum_{i=1}^{i}\left(\sum_{j=1}^{J}\left(\sum_{k}^{K}\left(\sum_{q}^{Q} \mathrm{AD}_{ij}(k,q)\right)\right)\right)}{K \cdot Q \cdot J \cdot i} \tag{3.7}$$

The expressions of D_{ri} and D_{r+i} in equitation (3.6)-(3.7) are valid for a perfect surface, i.e., for $\forall \mathrm{BD}_{ij}(k,q) = 0$, only.

However for determining D_r for a real surface one needs to see whether or not a cell is dressed. This can be determined by testing whether or not "$\mathrm{BD}_{ij}(k,q) \neq \mathrm{AD}_{ij}(k,q)$" is true. If "$\mathrm{BD}_{ij}(k,q) \neq \mathrm{AD}_{ij}(k,q)$" is true then the cell has been dressed. This yields the following parameter.

$$\mathrm{RD}_{ij}(k,q) = \begin{cases} 1 & \mathrm{BD}_{ij}(k,q) \neq \mathrm{AD}_{ij}(k,q) \\ 0 & otherwise \end{cases} \tag{3.8}$$

As such, the counter $\mathrm{RD}_{ij}(k,q) \in \{0, 1\}$ defined in equation (3.8) can be used to

determine D_{ri} and D_{r+i} for real surface. The expressions are as follows:

$$D_{ri} = \frac{\sum_{j=1}^{J}\left(\sum_{k}^{K}\left(\sum_{q}^{Q} \mathrm{RD}_{ij}(k,q)\right)\right)}{K \cdot Q \cdot J} \tag{3.9}$$

$$D_{r+i} = \frac{\sum_{i=1}^{i}\left(\sum_{j=1}^{J}\left(\sum_{k}^{K}\left(\sum_{q}^{Q} \mathrm{RD}_{ij}(k,q)\right)\right)\right)}{K \cdot Q \cdot J \cdot i} \tag{3.10}$$

However, a cell could be dressed twice or more. This can be verified by comparing $\mathrm{AD}_{ij}(k,q)$, $\mathrm{AD}_{ij+1}(k,q)$, and so on in a given pass. Thus, the records $\mathrm{AD}_{ij}(k,q)$ of all trajectories should be added to see whether or not a cell is dressed more once. To determine this first consider a counter as follows:

$$\mathrm{AD}_i(k,q) = \sum_{j=1}^{J} \mathrm{AD}_{ij}(k,q) \tag{3.11}$$

As such, $\mathrm{AD}_i(k,q) \in \{0, 1, 2,...\}$. If $\mathrm{AD}_i(k,q) = 2$ then the cell has been dressed twice. If $\mathrm{AD}_i(k,q) = 3$ then the cell has been dressed thrice. In general, if $\mathrm{AD}_i(k,q) = M$ ($\in \aleph$), then the cell has been dressed M times. This yields a counter given as

$$\mathrm{MD}_{Mi}(k,q) = \begin{cases} 1 & \mathrm{AD}_i(k,q) = M \\ 0 & otherwise \end{cases} \tag{3.12}$$

As such, the counter $\mathrm{MD}_{Mi}(k,q) \in \{0, 1\}$ defined in equation (3.12) can be used to determine D_{rMi} (i.e., dressing ratio of M times dressed area in i-th pass) and D_{rM+i} (i.e., dressing ratio of M times dressed area up to i passes) for ideal surface. The expressions are as follows:

$$D_{rMi} = \frac{\sum_{k}^{K}\left(\sum_{q}^{Q} \mathrm{MD}_{Mi}(k,q)\right)}{K \cdot Q} \tag{3.13}$$

$$D_{rM+i} = \frac{\sum_{i=1}^{i}\left(\sum_{k}^{K}\left(\sum_{q}^{Q} \mathrm{MD}_{Mi}(k,q)\right)\right)}{K \cdot Q \cdot i} \tag{3.14}$$

Similar quantifiers can be defined for the other option (real surface), too.

Requirement 8: Requirement 8 means displaying the necessary inputs and outputs by both textural and graphical means. To fulfill this requirement a user-interface should be created wherein the user can input and display the parameters associated with requirements 1-3. The interface should also display the dressing trajectories for each passes and dressing ratio so as to provide visual feedback for users to take necessary action to improve the dressing performance.

3.2. Outline of the Proposed Simulation System

The previous section describes eight requirements that are essential to achieve the proposed system. These requirements are listed in Table 3.1.

Table 3.1. Summary of the requirements of the proposed simulation system

Requirement 1	Setting the surfaces for simulation and calculation
Requirement 2	Determining the geometry of dressing trajectory
Requirement 3	Determining the orientation of the trajectories
Requirement 4	Determining the offset
Requirement 5	Determining the coordinates of the starting point of a pass
Requirement 6	Digitizing the effect of each dressing trajectory belonging to the boundary of RS

Table 3.1 continues	
Requirement 7	Determining the dressing ratio
Requirement 8	Displaying the necessary inputs and outputs by both textural and graphical means

As listed in Table 3.1, the requirements are as follows: 1) setting the surfaces for simulation and calculation; 2) determining the geometry of the dressing trajectory; 3) determining the orientation of the trajectories; 4) determining the offset; 5) determining the coordinates of the starting point of a pass; 6) digitizing the effect of each dressing trajectory belonging to the boundary of RS; 7) Determining the dressing ratio; and 8) displaying the necessary inputs and outputs by both textural and graphical means. Figure 3.9 schematically illustrates the outline of the proposed simulation system. As seen from Fig. 3.9, the layout consists of eleven integrated modules. These modules are: 1) *parameter module* (related to requirement 2); 2) *trajectory geometry module* (also related to requirement 2); 3) *trajectory orientation module* (related to requirement 3); 4) *trajectory offset module* (related to requirement 4); 5) *starting point creation module* (related to requirement 5); 6) *trajectory creation module* (related to all requirements 1-5); 7) *initial surface setting module* (requirement 7); 8) *digitization module* (related to both requirement 1 (RS) and requirement 6); 9) *dressing ratio module* (related requirement 7); 10) *recursion module* (related to all requirements 1-8); and 11) *display module* (related to requirement 8 (i.e., user-interface). The modules 1-5 belong to a block denoted as A and shown by a dotted box in Fig. 3.9. On the other hand, the modules 6-9 belong to a block denoted as B and shown by the other dotted box in Fig. 3.9. The modules 10 and 11 are out of these blocks, however. The interactions among these modules are shown by some lines and numbers (1,...,10). The block A (i.e., modules 1-5), the modules 6, 7, and 9 interact with the display module (module 11).

These interactions are shown by the number 7 in Fig. 3.9. The recursion module (module 10) repeats the trajectory creation process for multiple passes and the calculation processes in other related module. Therefore, this module needs to interact with the blocks A and B and display module, as well. These interactions are shown by the number 10 in Fig. 3.9. Here, the user set whether or not the depth of cut remains constant for all passes or increase/decrease in different passes. For a single pass case, however, the recursion module remains inactive.

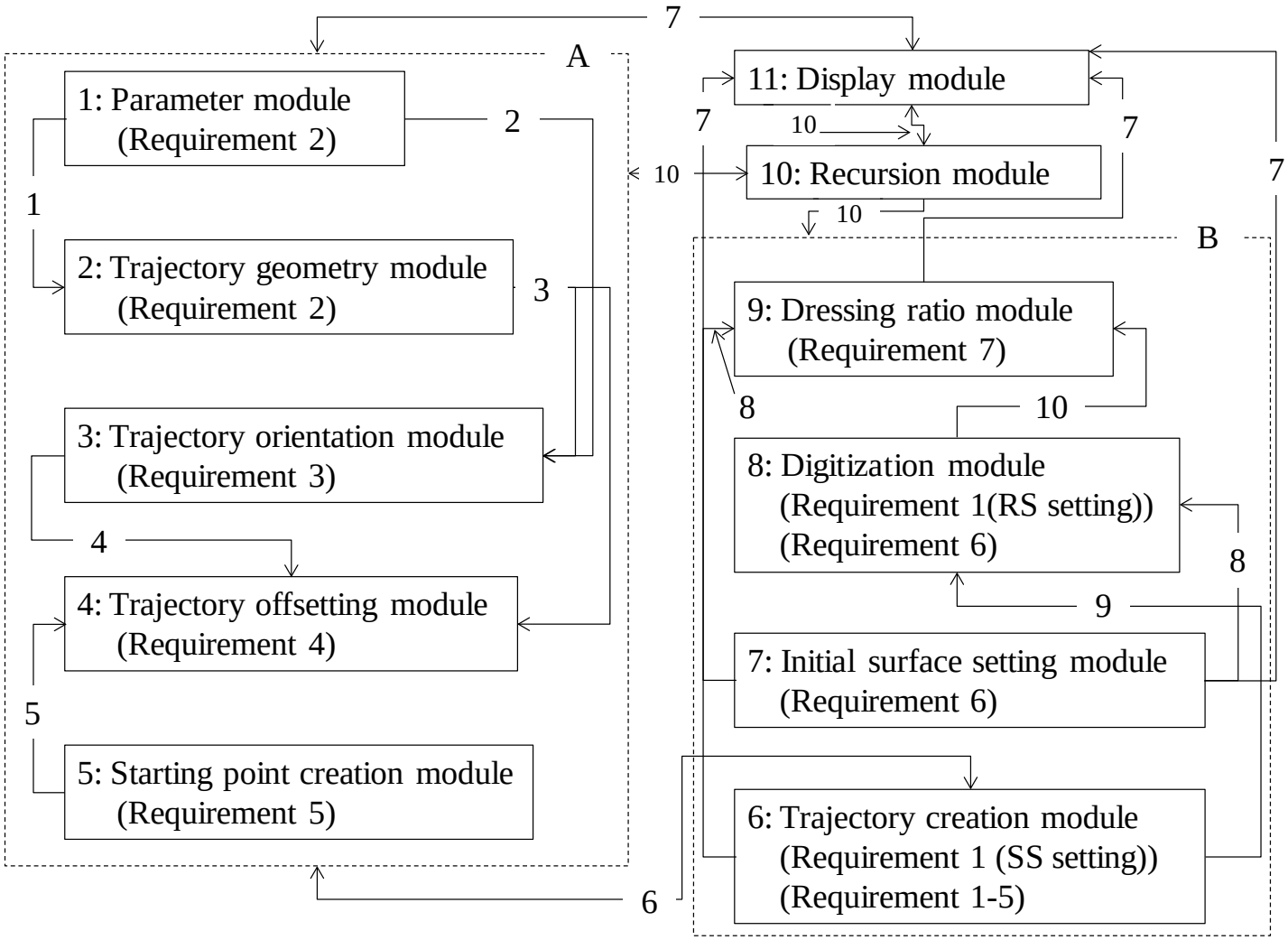

Figure 3.9. Outline of the proposed simulation system.

The interactions among the modules in the block A is described as follows. When the user sets the independent parameters related to parameter module through the display module, the results are used by the trajectory geometry module (interaction 1) and trajectory orientation module (interaction 2). The outcomes of the trajectory geometry module are used by the trajectory orientation module (interaction 3) and trajectory offsetting module (interaction 4). The starting point creation module interacts with the trajectory offsetting module (interaction 5). The interactions among the modules in the block B are as follows. All these interactions are also related to the trajectory creation process (interaction 6). When user sets the input for the initial surface setting module (module 7) through the display module (iteration 7), the module 8 (digitization module) is activated as indicated by the interaction 8. At the same time, the information is also shared by the dressing ratio module as indicated by the same interaction number 8. The dressing ratio module also interacts with the digitization module (interaction 10).

A simulation system can be developed using a suitable programming platform. Irrespective of the platform, the needs the abovementioned modules (modules 1,...,11) and the interactions 1,...,10. This issue is discussed in the next section.

3.3. The Proposed Simulation System

The user interface (display module or module 11, in Fig. 3.9) of the simulation system is shown in Figs. 3.10-11. The system has been developed by using the spreadsheet application called Excel™. This system is hereinafter referred to as DSys (Dressing Simulation System). The section describes the operating principles DSys.

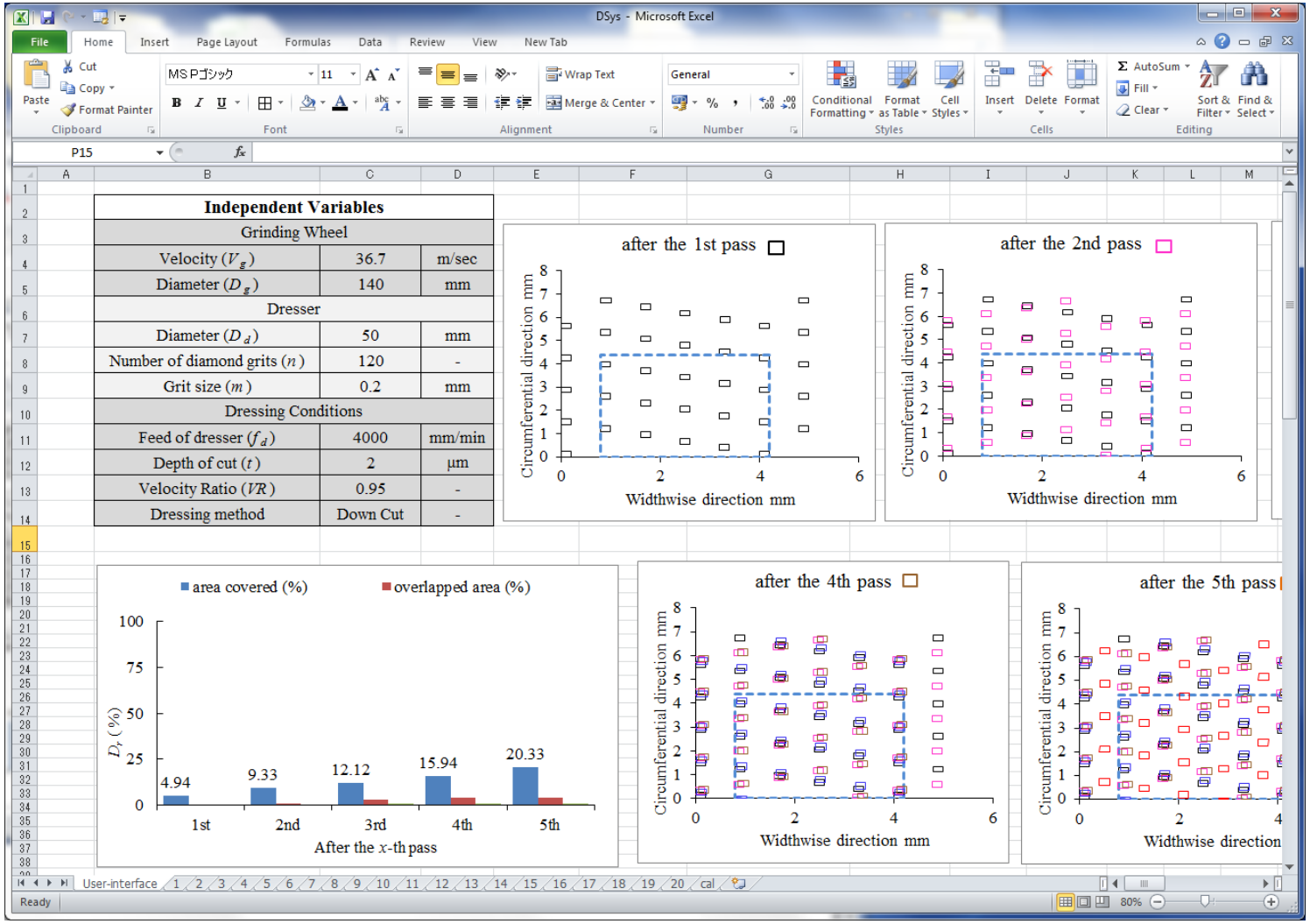

Figure 3.10. A screenshot of DSys for down-cut.

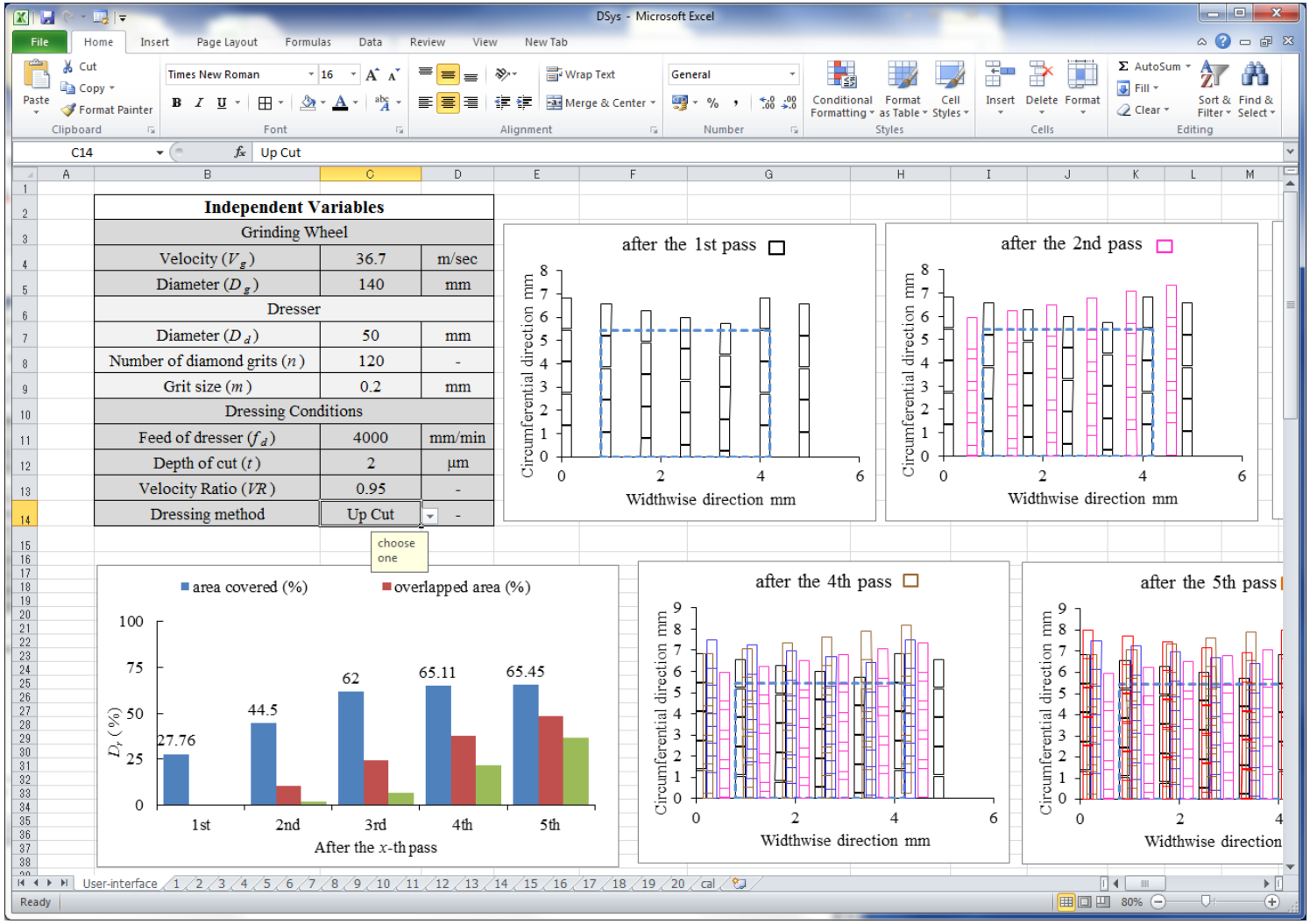

Figure 3.11. A screenshot of DSys for up-cut.

The simulation system requires a set of independent variables which are to be set as inputs of the system: Diameter of grinding wheel D_g, Diameter of rotary diamond dresser D_d, Peripheral speed of grinding wheel V_g, Number of diamond grits on rotary diamond dresser n, Length of diamond grits on rotary diamond dresser m, Width of diamond grits on rotary diamond dresser D_b, Feed speed of rotary diamond dresser f_d, Depth of cut in dressing t, Velocity ratio of rotary diamond dresser to grinding wheel (V_d / V_g) VR, Number of passes in dressing N_D and the dressing method: Up-cut or Down-cut dressing. $N_D = 1$ corresponds to single-pass dressing. Using the set of inputs, the parameters: Length of dressing trajectory l_a , Pitch of dressing trajectory P, Gap between two successive trajectories g, Dressing lead (f_d / N_g) L_d and Lead angle of dressing θ are calculated. In second step, a series of dressing trajectories are formed on the grinding wheel surface using the calculated parameters in accordance with the requirements 1-6 described in section 3.1-2 (as illustrated in Fig. 3.1). In the next step, the dressing ratio D_r, which is defined in requirement 7 of the section 3.1, is calculated. In the final step, the necessary inputs and outputs are displayed by both textural and graphical means as explained in requirement 8 of section 3.1. This procedure is performed N_D times. The results obtained for a given set of dressing conditions by using DSys are explained in the following two sections

3.3.1 Down-cut in Figure 3.9

Table 3.2 shows the independent variables, i.e., the inputs of the simulation system for the Down-cut method which are displayed in the DSys (refer to Fig. 3.10). In DSys, the grinding wheel surface after 1st pass, 2nd pass, 3rd pass, 4th pass and 5th pass of

Table 3.2. Inputs for the simulation system (dressing conditions)

Variables	Values/Conditions
D_g,V_g	140 mm, 36.7 m/s (5000 rpm), respectively
D_d	50 mm
n, m, D_b	120, 0.2 mm, 0.2 mm, respectively
t, N_D, Type of cut, VR, f_d	2 μm, multiple pass (5), Down-cut, VR=-0.95, 4000 mm/min respectively

RDD are displayed as outputs (refer to Fig. 3.10). Note that grinding wheel surface after 3rd pass of RDD is not shown in Fig. 3.10 due to space limitation of the page. It is clearly observed from the graphical means that the undressed area part is higher for the dressing conditions shown in Table 3.2. Furthermore, the textural display shows the Dressing ratio, D_r for the given dressing conditions (refer to Table 3.2). The textural display shows the percentage of dressed grinding wheel surface area after 5th pass of RDD which is only 20.33% of the total RS.

3.3.2 Up-cut in Figure 3.10

Table 3.3. Inputs for the simulation system (dressing conditions)

Variables	Values/Conditions
D_g,V_g	140 mm, 36.7 m/s (5000 rpm), respectively
D_d	50 mm
n, m, D_b	120, 0.2 mm, 0.2 mm, respectively
t, N_D, Type of cut, VR, f_d	2 μm, multiple pass (5), Up-cut, VR=+0.95, 4000 mm/min respectively

Table 3.3 shows the independent variables, i.e., the inputs of the simulation system for the Up-cut method which are displayed in the DSys (refer to Fig. 3.11). In DSys, the grinding wheel surface after 1^{st} pass, 2^{nd} pass, 3^{rd} pass, 4^{th} pass and 5^{th} pass of RDD are displayed as outputs (refer to Fig. 3.11). Note that grinding wheel surface after 3^{rd} pass of RDD is not shown in Fig. 3.11 due to space limitation of the page. It is clearly observed from the graphical display that the undressed area part is lower for the dressing conditions shown in Table 3.3 than that of dressing conditions shown in Table 3.2. Furthermore, the textural display shows the Dressing ratio, D_r for the given dressing conditions (refer to Table 3.3). The textural display shows the percentage of dressed grinding wheel surface area after 5^{th} pass of RDD which is 65.45% of the total RS. In these two dressing conditions, the only parameter that is different is the dressing method, i.e., Down-cut or Up-cut. Therefore, It can be stated by comparing these two results is that the length of the dressing trajectory is larger in case of Up-cut than that of Down-cut. Furthermore, It can be concluded that more dressed grinding wheel surface area can be realized by Up-cut compared to Down-cut.

Chapter 4
2D Dressing Performance

The grinding wheel surface topography after dressing is an indicator of the effectiveness of dressing operation and, thereby, the effectiveness of grinding as a whole. In this chapter, a computer-aided simulation is developed to generate the two dimentional surface topography of grinding wheel after dressing considering the perfect grinding wheel surface. From the generated two dimentional topographies, one can determine the effectiveness of certain dressing conditions beforehand. In addition, the computer-aided simulation can be used for optimizing the design variables of a rotary diamond dresser. This chapter is based on the work of Chowdhury et al. [32,36]. For better understanding this chapter is structured into the following sub-sections: Dressed Patterns, Effect of Feed Rate in Single-pass Dressing, Effect of number of passes in multipass Dressing, Relation of Number of Passes Required for Complete Dressing with Depth of Cut.

4.1 Dressed Patterns

Using the inputs (refer to Table 2.2) of the user interface (refer to Fig. 3.10), the simulation generates the two-dimensional topographies of the grinding wheel surface for several passes of dresser in accordance with the outline of proposed simulation system (refer to Fig. 3.9) and defined in sections 3.1-2 considering the perfect grinding wheel surface ($z = 0$).

Figure 4.1 shows examples of dressed patterns obtained from the dressing simulations carried out for a diamond grit width D_b of 0.2 mm, a depth of cut t of 2 μm and a dressing lead L_d of 0.4 mm/rev. It can be seen that continuous dressing trajectories are formed at VR = +1.2 and that separated dressing trajectories are formed at VR = +0.7 and +0.5. Note that these results are derived from Fig. 2.8, which shows the critical depth of cut. For example, the critical depth of cut in dressing at VR = +1.2 is 1.7 μm, which is 0.3 μm smaller than the depth of cut, t =2 μm. This result indicates that continuous dressing trajectories are formed at VR = +1.2.

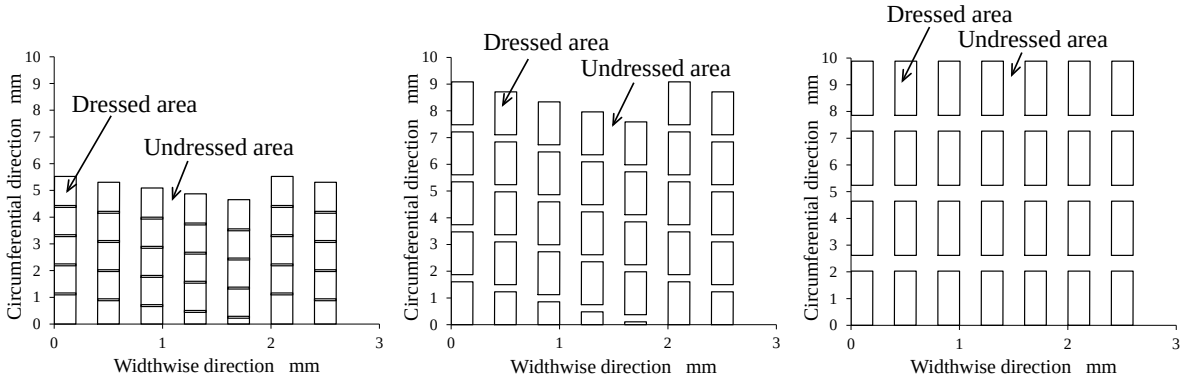

(a) VR = +1.2 (b) VR = +0.7 (c) VR = +0.5

Figure 4.1. Dressed pattern in single-pass dressing (D_b = 0.2 mm, L_d = 0.4 mm/rev., t = 2 μm).

Comparing the two dressed patterns for of VR = +0.7 and +0.5, it is found in the case of VR = +0.5 that every dressed area is located at the same circumferential position of the grinding wheel, regardless of the width direction of the grinding wheel, namely, there is no offset of the dressing trajectory which is shown in Fig. 2.2. This is because the pitch of the dressing trajectories P divides into the circumference of the grinding wheel πD_g at VR = ±0.5. The quotient is calculated to

be 168 in this case.

By investigating the dressing lead L_d that realizes complete dressing, i.e., D_r =1, the following dressing strategies are found. In the case where continuous dressing trajectories are formed (see Fig. 4.1 (a)), compete dressing can be realized by setting L_d to the same value as the width of the diamond grit D_b. In the case where the separated dressing trajectories have an offset (see Fig. 4.1 (b)), complete dressing is realized by setting L_d to a value less than D_b so that the series of dressing trajectories overlap with each other. However, in the case where the separated dressing trajectories have no offset (see Fig. 4.1 (c)), L_d cannot be tuned to achieve the complete dressing.

4.2 Effect of Feed Rate in Single-pass Dressing

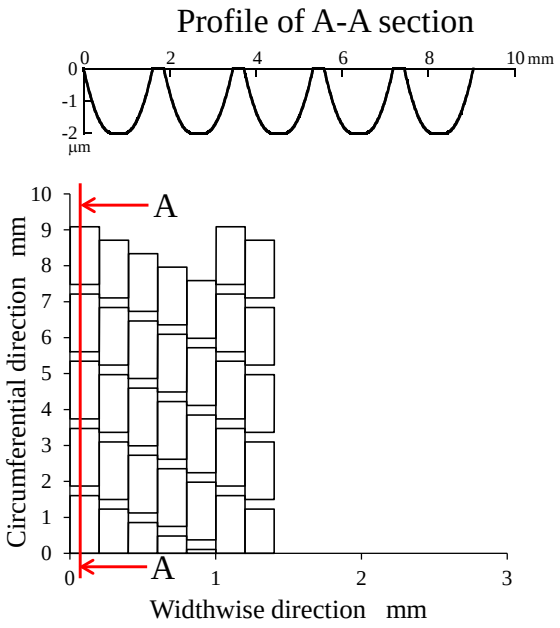

(a) $FR = 1$

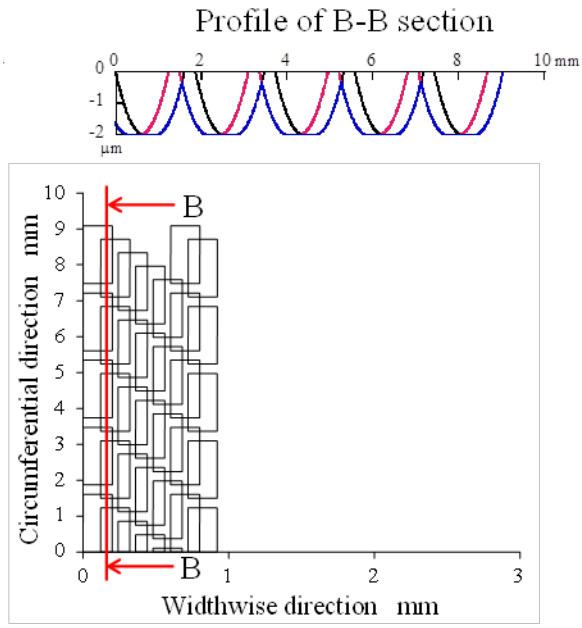

(b) $FR = 0.6$

Figure 4.2. Effect of *FR* on the dressed surface in single-pass dressing (*VR* = +0.7, *t* = 2 μm).

As a parameter to evaluate the effect of the dressing lead on the dressing ratio, the dresser feed rate *FR* is defined as

$$FR = \frac{L_d}{D_b} \tag{4.1}$$

Figure 4.2 shows the change in the dressed pattern formed on the grinding wheel surface when *FR* is changed from 1 to 0.6. The dressing conditions are the same as those for Fig. 4.1 (b), and the dressed pattern shown in Fig. 4.1 (b) corresponds to the result for *FR* = 2. It can be seen from the figure that the area of the undressed parts decreases with decreasing *FR*.

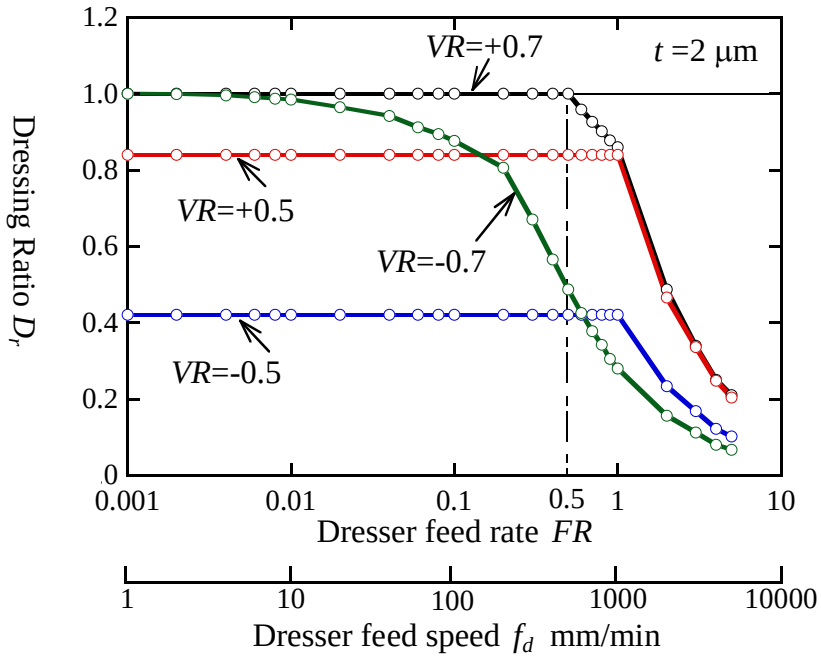

Figure 4.3. Dressing ratio vs. dresser feed rate in single-pass dressing at t = 2 μm.

Figure 4.3 shows plots of the dressing ratio D_r against FR for various values of VR. As mentioned before, complete dressing, i.e., D_r = 1, is not achieved when VR = ±0.5. On the other hand, complete dressing is achieved for FR = 0.5 when VR = +0.7, and for FR = 0.001 when VR = - 0.7. In the figure, FR = 0.5 and 0.001 correspond to dresser feed speeds of 500 and 1 mm/min, respectively. The dresser feed speed of 500 mm/min is a value set in actual dressing; therefore, it can be concluded that complete dressing is realized in the case of up-cut dressing with VR = +0.7 if the dresser feed speed of the RDD is set at 500 mm/min. However, in the case of down-cut dressing with VR = - 0.7, the dresser feed speed of 1 mm/min is too slow to realize using practical dressing apparatus; therefore complete dressing is almost impossible to achieve.

4.3 Effect of Number of Passes in Dressing

Multipass dressing is applied for dressing using small depth of cut which minimize the dressing force and consequently deformation. Number of passes is an important parameter in this type of dressing for achieving dressing efficiency.

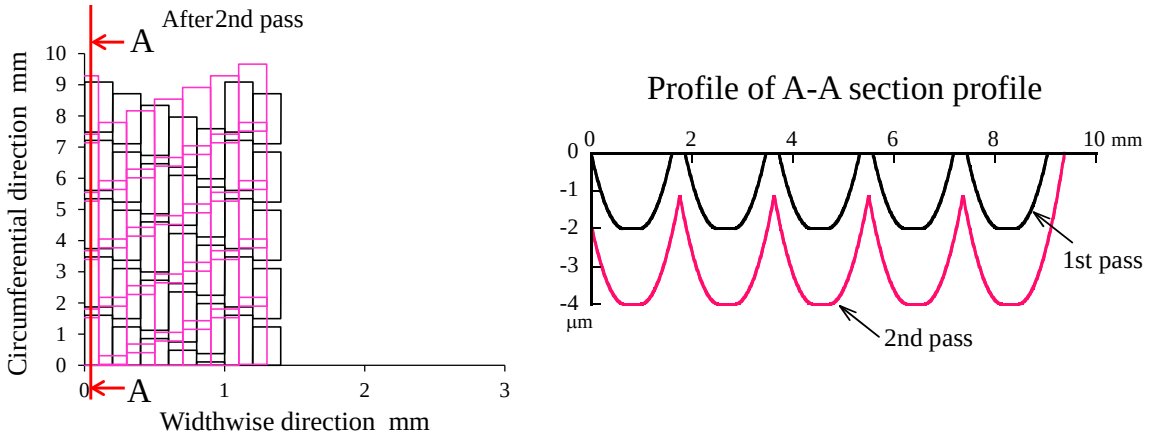

Figure 4.4. Dressed surface after 2nd pass dressing (*VR* = +0.7, *t* = 2 μm, *FR* =1).

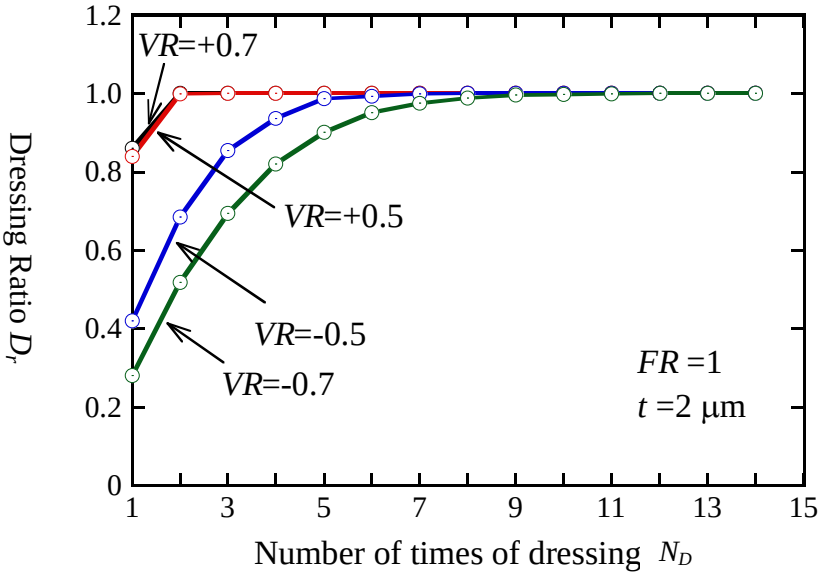

Figure 4.5. Dressing ratio vs. number of times of dressing (*t* = 2 μm, *FR* =1)

Figure 4.4 shows the dressed pattern formed on the grinding wheel surface after two passes, i.e., N_D = 2. The dressing conditions are the same as those for Fig. 4.1 (b) except for FR = 1. A depth of cut of t = 2 μm was given for each pass on both side edges of the grinding wheel. The dressed pattern shown in Fig. 4.2 (a) corresponds to the result for N_D = 1. It can be seen from the figure that the undressed area almost disappears after two-pass dressing. The profile at A-A section reiterates the statement of disappearance of most undressed part, wherein the depth of cut is increased in the 2nd pass.

Figure 4.5 shows plots of D_r against N_D. It can be seen from the figure that the number of passes that realizes the complete dressing, i.e., D_r = 1, is three in the cases of up-cut dressing with VR = +0.5 and +0.7, and 8 and 14 in the cases of down-cut dressing with VR = -0.5 and -0.7, respectively. The reason why a higher number of passes is required to achieve complete dressing in the case of down-cut dressing is that the contact length of the dressing trajectory in down-cut dressing is markedly smaller than that in up-cut dressing (see Figs. 2.6 and 2.7), although the pitch of the dressing trajectory given by Eq. (11) takes the same value in up-cut dressing and down-cut dressing for a given value of VR.

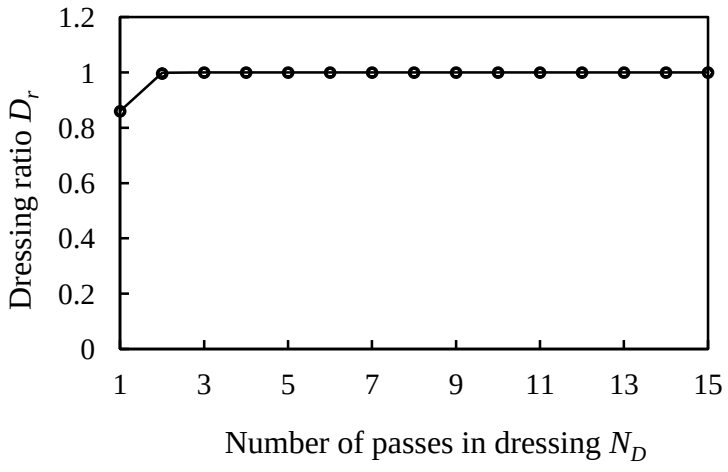

Figure 4.6. Variation of dressing ratio for random starting points in up-cut (FR=1, VR=+0.7, No of Simulation=100).

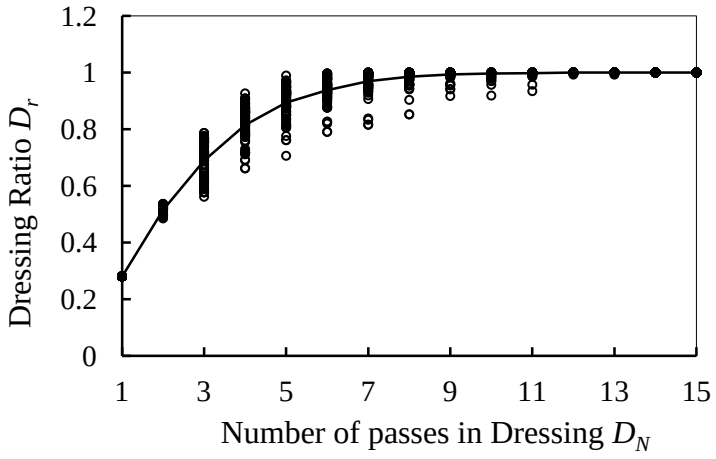

Figure 4.7. Variation of dressing ratio for random starting points in down-cut (*FR*=1, *VR*=-0.7, No of Simulation=100).

In the case of multipass dressing, the RDD comes into contact with the grinding wheel surface at an arbitrary position at each dressing pass (as illustrated in Section 2.2); therefore, the starting point of a series of dressing trajectories should be given at random in the simulation. This indicates that the grinding wheel surface topography is affected by the starting point of the dressing trajectories in multipass dressing. Taking this into consideration, the dressing simulation was carried out 100 times and Figure 4.6 and 4.7 are drawn. From Figs. 4.6 and 4.7, it can be seen that the effect of random start points on D_r is markedly observed in down-cut dressing than that of up-cut dressing. The reason is that the gap between the two consecutive dressing trajectories is larger in down-cut than that in up-cut.

4.4 Relationship between Number of Passes and Depth of Cut for Complete Dressing

The complete dressing D_c is realized when the diamond grits of the RDD come in contact with the entire working surface of the grinding wheel. Figure 4.8(a) shows the number of passes required for D_c against depth of cut *t*. It can be seen that

the required number of passes that realizes D_c deceases with the increase in t. It is also seen that for FR=1, when VR=+0.7 (up-cut) and t=2μm it realizes complete dressing after two passes of dresser. From Fig. 4.8(a) it can be concluded that complete dressing is realized by lesser number of passes in case of up-cut than that in down-cut dressing.

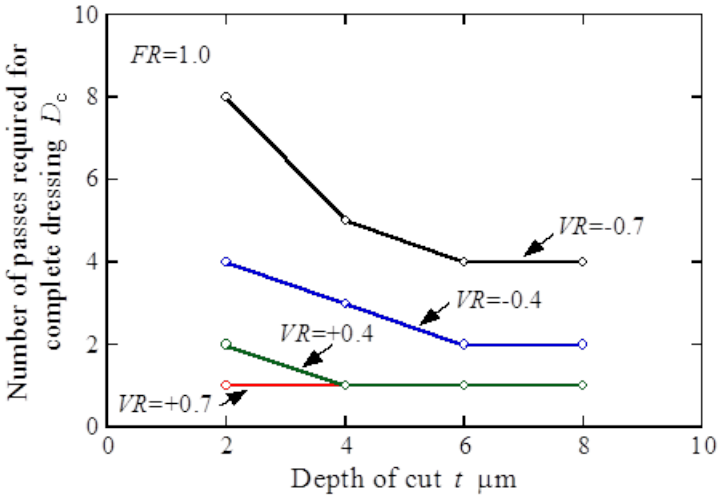

(a) Number of passes vs. depth of cut

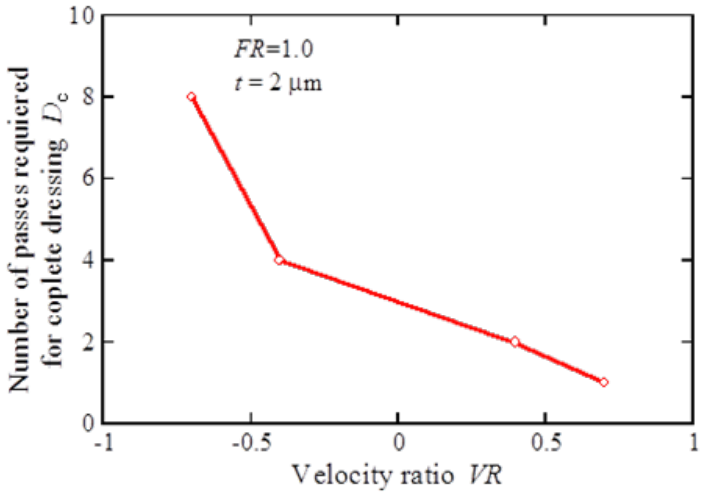

(b) Number of passes vs. velocity ratio

Figure 4.8. Number of passes required for complete dressing.

Figure 4.8(b) shows the number of passes required for D_c is 6 times when VR=-0.5 and 2 times when VR=+0.5. Therefore, it can be reiterated that lesser number of passes is required for realizing complete dressing in up-cut than that in down-cut dressing due to the gap between two dressing trajectories is smaller in up-cut dressing than that in down-cut dressing.

Chapter 5
3D Dressing Performance

This chapter deals with the 3D dressing performance analysis. In the previous chapter the dressing performance (the degree of dressed area) is determined based on dressing trajectories on the plane $z = 0$. A dressing trajectory has a sectional profile. This means that the presence of dressing trajectory in the depth-wise direction (sectional profile) is an important aspect of dressing performance analysis. At the same time, the outermost surface of a grinding wheel is not a smooth surface. This means that $z = 0$ does not represent a real grinding wheel surface. Therefore, it is important to revisit the results described in Chapter 4 from the perspectives of both the effect of sectional profile dressing trajectory and surface profile of grinding wheel. Accordingly, this chapter is organized as follows. Section 5.1 describes the perspective of surface profile of grinding wheel. Section 5.2 describes the perspective of sectional profile of dressing trajectory with regard to surface profile of grinding wheel. Section 5.3 describes the dressing performance based on surface profile of grinding wheel and evectional profile of dressing trajectory.

5.1. Surface Profile of Grinding Wheel

The surface profile of grinding wheel is highly irregular (Yamaguchi et al. [37], Ullah et al. [38]). In particular a grinding wheel is fabricated by bonding abrasive grains. Figure 5.1 schematically illustrates the bonded abrasive grains of a grinding wheel.

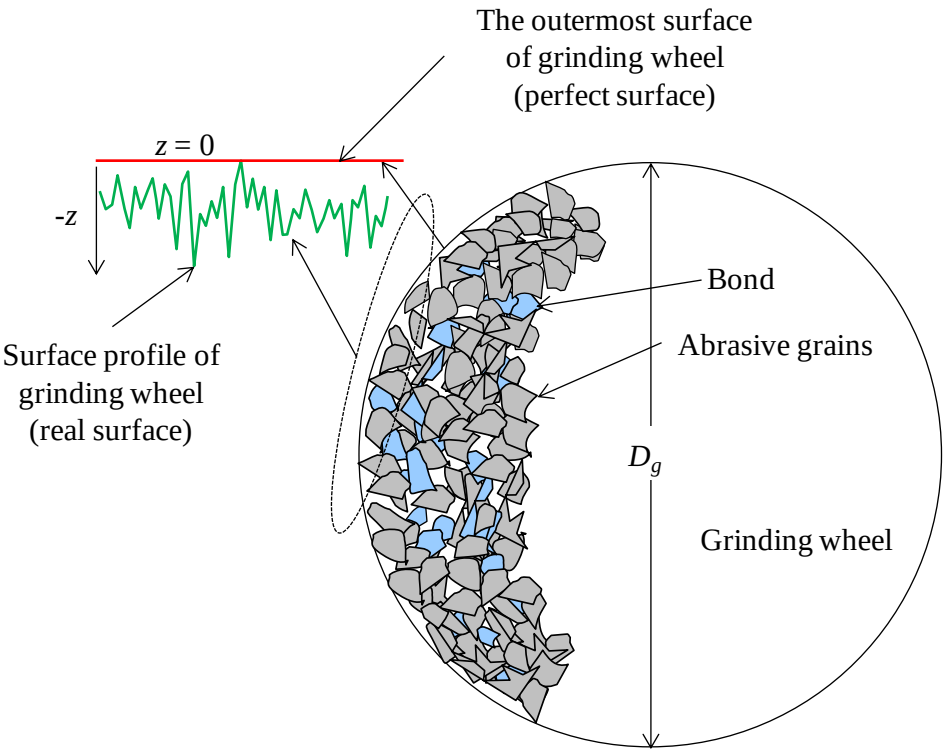

Figure 5.1. A model of grinding wheel.

As seen from Fig. 5.1, the irregular orientations of the abrasive grains produce an ever varying height of the outermost surface of grinding wheel. This irregularity can be represented by a surface profile. The maximum height of the profile is $z = 0$ that represent the outermost boundary of a grinding wheel having a diameter of D_g. Other than the maximum height, $z < 0$. Therefore, the z-coordinates of the points on the

surface profile are all equal to 0 correspond to a case called perfect surface profile of grinding wheel (the red line in Fig. 5.1). On the other hand, the z-coordinates of the points on the profile are $z_{rpi} \leq 0$, $i = 1,2,...$ correspond to a case called real surface profile of grinding wheel (the green profile in Fig. 5.1). To simulation a real surface profile one can use stochastic processes can be used (Yamaguchi et al. [37]; Ullah et al. 2010 [38]), however. In this study, an stochastic approach based on the average grain size is used. The approach is schematically illustrated in Fig. 5.2.

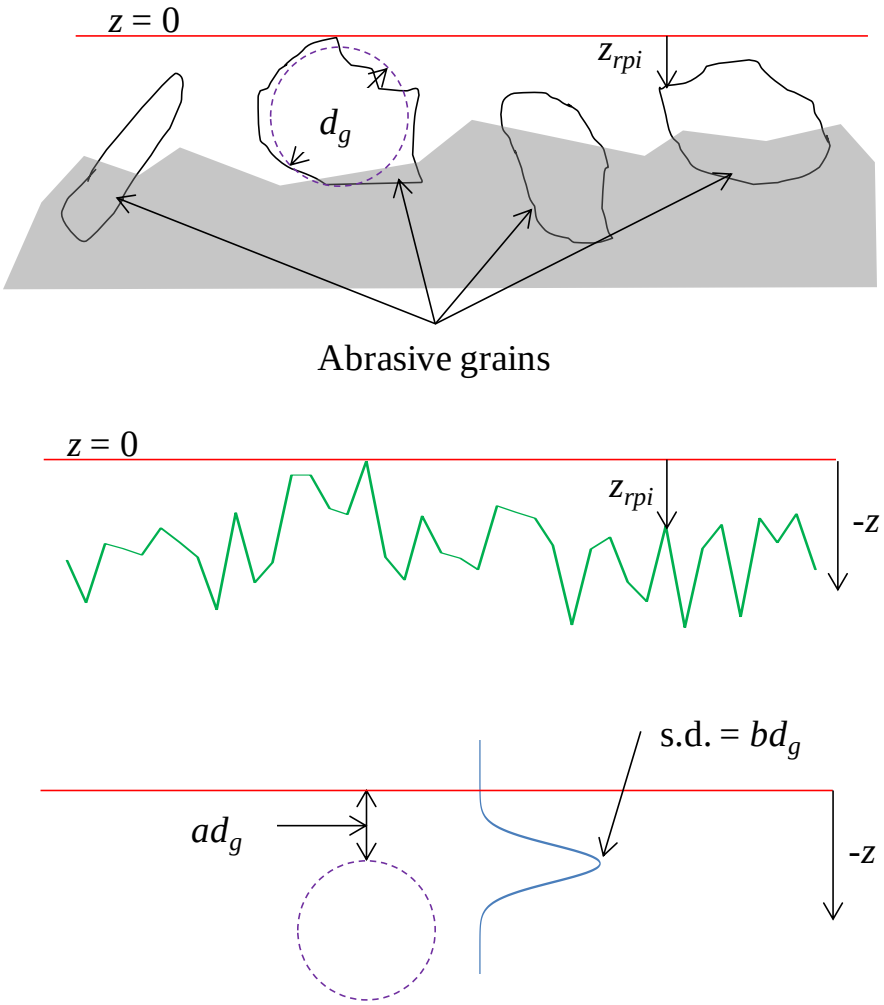

Figure 5.2. Simulation of real surface profile of grinding wheel.

It has been observed that the grain size (i.e., actual value of d_g) is normally

distributed. For the sake of simulation it can be assumed that the expected position of the tip of an ideal grain is $-ad_g$ whereas the variability in the size/placement of the grain is taken care of by the standard deviation bd_g. Here a and b are two user-defined constants. Thus, the simulated height of a real surface profile z_{rpi} (i = 1,2,..., (the index i represents a simulation instance) is a normally distributed variable with mean $-ad_g$ and standard deviation bd_g as schematically illustrated in Fig. 5.2. At the same time, it is also true that z_{rpi} does not exceed the limit z = 0, i.e., the outermost boundary of the grinding wheel. Based on this assumption the following formation of z_{rpi} is proposed

$$z_{rpi} = \min\left(0, nv_i\left(-ad_g, bd_g\right)\right) \tag{5.1}$$

In equation (5.1), the index i denotes a simulation instance, $nv_i(-ad_g,bd_g)$ denotes a normally distributed random variable having a mean $-ad_g$ and standard deviation bd_g, d_g is the average grain size of the abrasives, a, $b \in (0,1]$ are two user-defined constants, and z_{ai} is the simulated height of the real surface profile of grinding wheel. The setting in equation (5.1) ensures that the simulated height $z_{rpi} \leq 0$.

When no other information is supplied regarding the real surface profile, $a = b = 0.5$. This convention is followed in this study. Figure 5.3 shows a plot of z_{rpi} for d_g = 10 μm and $a = b = 0.5$. As seen from Fig. 5.3, the condition $z_{rpi} \leq 0$ has been achieved by the formulation in equation (5.1).

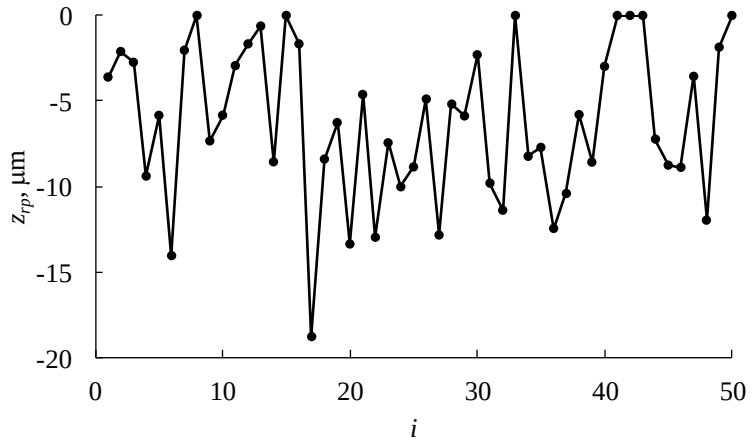

Figure 5.3. Simulated real surface profile height of grinding wheel.

5.2. Sectional Profile of Dressing Trajectory

The sectional profile of dressing trajectory has been defined in equation (2.13). The general characteristics of the section profile have also been described in Section 2.3 (see Fig. 2.4). For the sake of better understanding, two sectional profiles are shown by the 3D plots in Fig. 5.4. The sectional profile in Fig. 5.4(a) corresponds to f_d = 505 mm/min, L_d = 0.1 mm/rev, FR = 0.5, VR = +0.8, whereas the other corresponds to f_d = 2020 mm/min, L_d = 0.4 mm/rev, FR = 2, VR = +0.7. See Table 5.1 for other conditions.

Table 5.1. The conditions of dressing for 3D representation.

Variables	Values/Conditions
D_g,V_g	140 mm, 36.7 m/s (5000 rpm), respectively
D_d	50 mm
n, m, D_b	120, 0.2 mm, 0.2 mm, respectively
t, ND, Type of cut	2 μm, single pass, Up-cut (i.e., +VR), respectively

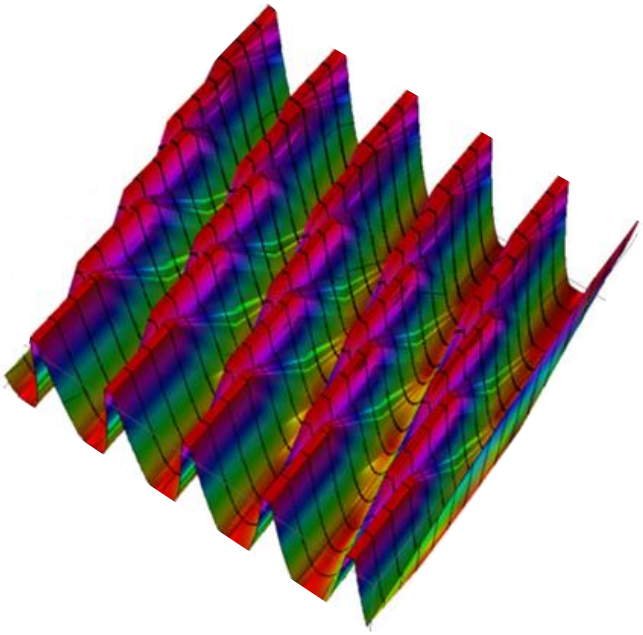

(a) f_d = 505 mm/min, L_d = 0.1 mm/rev, FR = 0.5, VR = +0.8

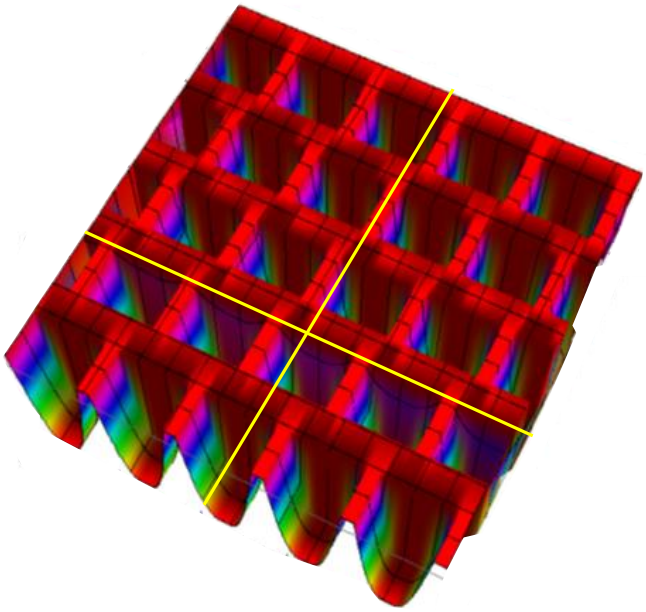

(b) f_d = 2020 mm/min, L_d = 0.4 mm/rev, FR = 2, VR = +0.7

Fig. 5.4. 3D representation of the sectional profile of dressing trajectory.

As seen from Fig. 5.4 a complex shape is created when the sectional profile of dressing trajectory is considered. To understand the nature of the shape creased in multiple passes is schematically illustrated in Fig. 5.5.

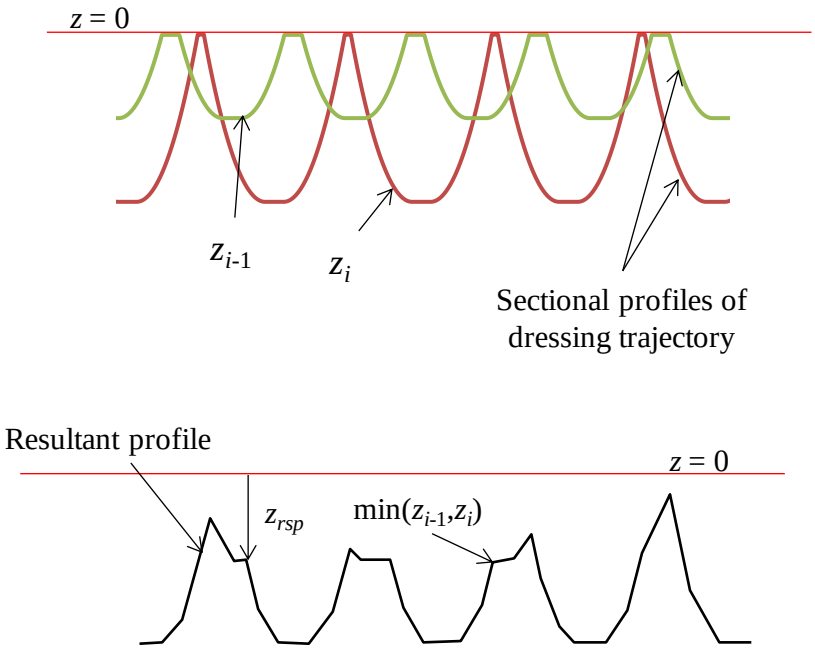

Figure 5.5. Resultant sectional profile.

As seen from Fig. 5.5, the depth of cut is increased every after each pass in multi-pass dressing. Compare the depth of the sectional profile of the (i-1)-sh pass and the i-th (i = 2,3,...) as shown in Fig. 5.5. In fact, the area occupied by the sectional profiles of the (i-1)-sh pass is not available during the i-th. The means that the minimum height of the section profiles of two consecutive passes, denoted as $\min(z_{i-1},z_i)$ determines the actual height of the section profile in the case of multiple passes. This creates a concept called resultant sectional profile. Thus, the height of the resultant sectional profile is given as

$$z_{rsp} = \min(z_{i-1}, z_i) \tag{5.2}$$

In equation (5.2), $z_{i\text{-}1}$ and z_i represent the heights of the sectional profile for the depth of cuts denoted as t_i-1 and t_i respectively. It is worth mentioning that the height of the sectional profile is considered in the direction of dressing defined by L_d and θ as described in Chapters 2 and 3. The height is slightly different in the circumferential or widthwise direction, however.

One noteworthy characteristic is that when D_r = 1 (a case of complete dressing in accordance with the results in Chapter 4), z_{rsp} remains well below z = 0 plane. The probability of getting $z_{rsp} \cong -t_i$ is very high compared to the point in the near z = 0. Therefore, when no other information is not available, the probability of height of the resultant sectional profile can be given by a triangular probability density function as follows:

$$\Pr(|z_{rsp}|) = \frac{2\, z_{rsp}}{(t_i)^2} \tag{5.3}$$

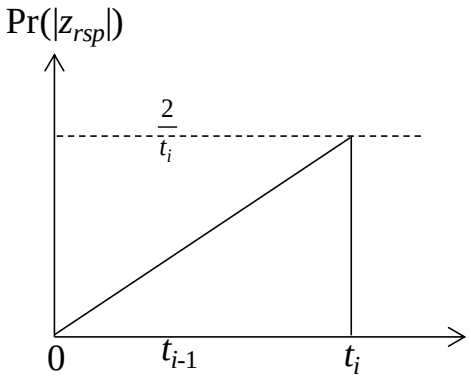

Figure 5.6. Triangular probability density function of the resultant sectional profile.

This function is illustrated in Fig. 5.6. As seen from Fig. 5.6, the maximum probability of z_{rsp} is near the depth of cut t_i and it decreases linearly with the decrease in $|z_{rsp}|$. Therefore, a random variable *tv* that follows the distribution of equation (5.3) can be used to simulate z_{rsp}. This yield the following equation.

$$z_{rspj} = -tv_j \tag{5.4}$$

In equation (5.4), the index *j* represents the *j*-th simulation instance and tv_j is the value of the random variable that follows the triangular probability distribution of equation (5.3), and z_{rspj} is the *j*-th simulated resultant sectional profile. The typical nature of the simulated resultant profile is shown in Fig. 5.7 that corresponds to t_i = 4 μm.

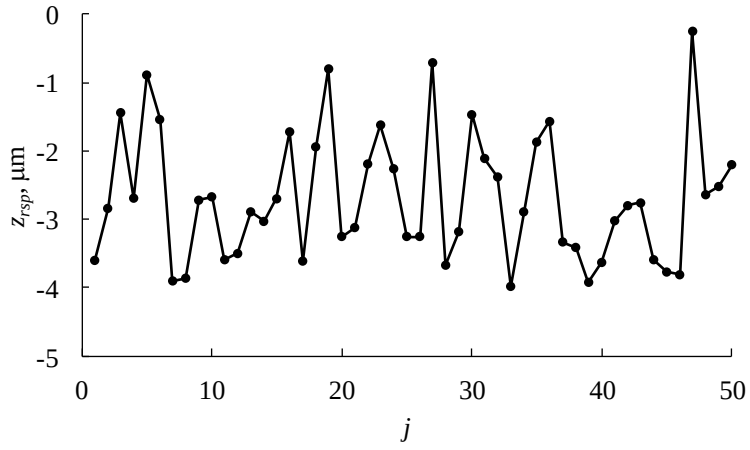

Figure 5.7. Simulated resultant sectional profile in accordance with equation (5.4).

One of the problems underlying the simulated resultant profile (Fig. 5.7) is that the points do not settle in the bottom (at a depth $-t_i$) as it should be compared to the real one

(Fig. 5.5). To solve this problem, the random variable can be redefined as a random variable of a triangular distribution as shown in Fig. 5.8.

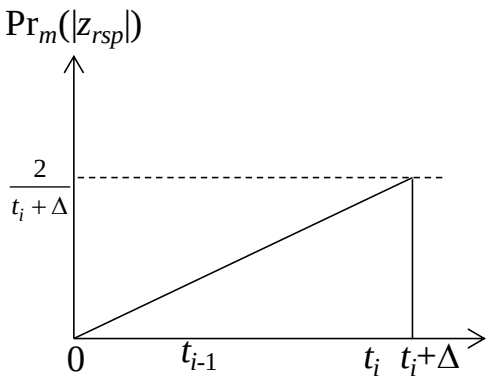

Figure 5.8. Modified triangular distribution of resultant sectional profile

In the case shown in Fig. 5.8, the triangular distribution is extended to $t_i+\Delta$. Therefore, this time the probability density function is given as

$$\Pr_m(|z_{rsp}|) = \frac{2\, z_{rsp}}{(t_i+\Delta)^2} \tag{5.5}$$

To make sure that the simulated resultant sectional profile does not exceed the limit, the following formulation can be used.

$$z_{rspj} = -\min(t_i, tv_{mj}) \tag{5.6}$$

In equation (5.6), the tv_{mi} follows the probability density function $\Pr_m(|z_{rsp}|)$ as defined in equation (5.5). The typical result of the simulated resultant sectional profile in accordance with equation (5.6) is shown in Fig. 5.9. The case shown in Fig. 5.9 corresponds to $\Delta = 2$. The choice of Δ depends on the number of passes. The more the

number of passes, the less the value of Δ. It also depends on the nature of the resultant sectional profile and also on the type of cut, however.

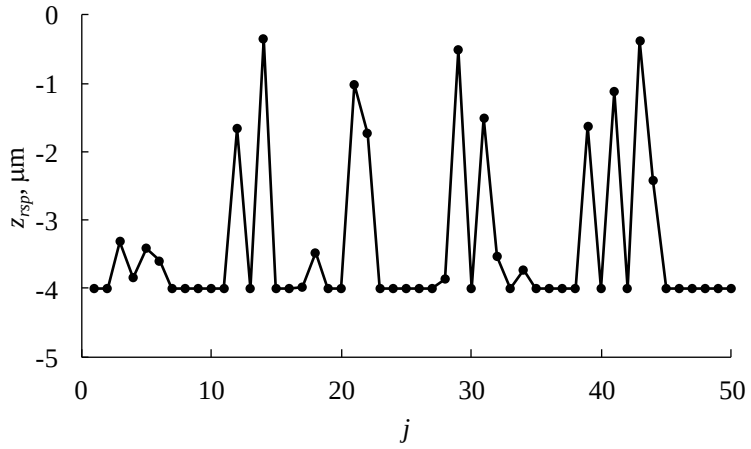

Figure 5.9. Simulated resultant sectional profile in accordance with equation ((5.6)).

5.3. Resultant Sectional Profile and Real Surface Profile of Grinding Wheel

Section 5.1 describes that the real surface profile of a grinding wheel and a method to simulate it. Section 5.2 describes the concept of resultant sectional profile of multiple passes and a method to simulate it. Therefore, it is important to see in general what happens when these two aspects (real surface profile of grinding wheel and resultant sectional profile) are considered simultaneously. One of the possibilities is schematically shown in Fig. 5.10. In Fig. 5.10, the outermost boundary of a grinding wheel (i.e., the case of perfect surface) is shown by a red line. The resultant sectional profile is shown by a black line, and the real surface profile of the grinding wheel is

shown by a green (irregular) line. The uppermost point of the real surface profile touches the outermost boundary of the grinding wheel.

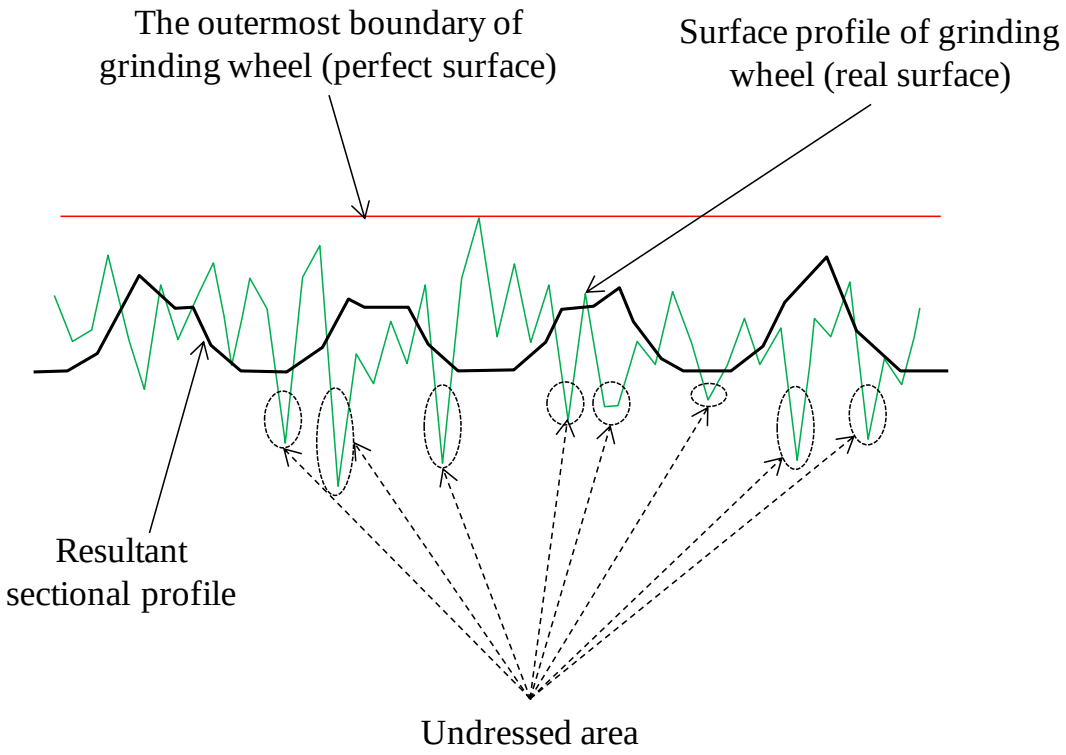

Figure 5.10. The interaction of resultant sectional profile and real surface profile grinding wheel.

One of the remarkable point is that there are real surface profile heights that are below the heights of the resultant sectional profile. As a result, the undressed areas as schematically illustrated in Fig. 5.10 come into being, even though the analyses based on the perfect surface profile (i.e., the results described in Chapter 4) confirm that a complete dressing has been achieved. How to find out the actual dressed area is an immediate question to answer. To answer this question, the procedure described in the requirement 6 and requirement 7 in Chapter 3 (Fig. 3.7) can be recalled.

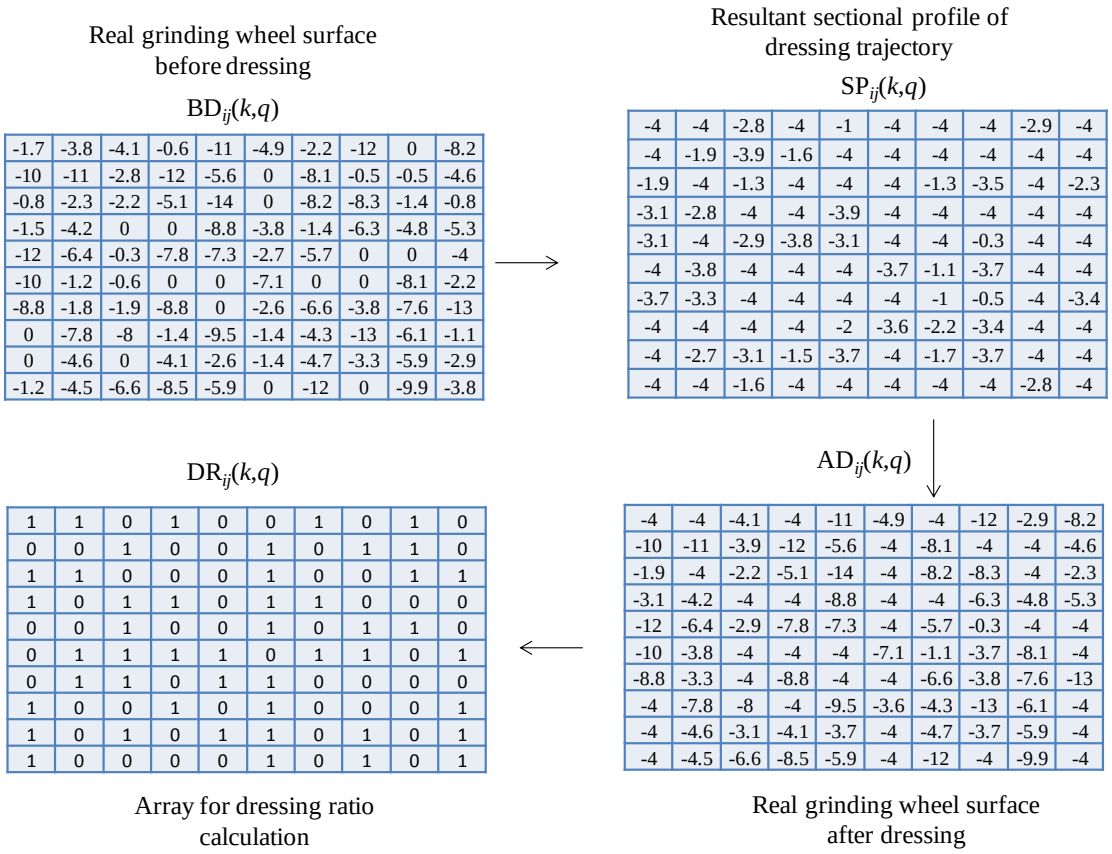

Figure 5.11.Digitization of RS based on real grinding wheel surface.

Figure 5.11 schematically illustrates digitization of dressed area RS based on real surface profile of grinding wheel for the dressing conditions listed in Table 5.2.

Table 5.2. The conditions of dressing for 3D representation.

Variables	Values/Conditions
D_g,V_g	140 mm, 36.7 m/s (5000 rpm), respectively
D_d	50 mm
n, m, D_b	120, 0.2 mm, 0.2 mm, respectively
t, N_D, Type of cut, VR, f_d	2 μm, after 2nd pass, Up-cut, VR=+0.7, 1010 mm/min respectively

The grinding wheel surface before dressing and simulated surface of the resultant sectional profile are achievable form the value of $BD_{ij}(k,q)$ and $SP_{ij}(k,q)$ respectively. The real 3D grinding wheel surface after dressing can be visualized after plotting the value of $AD_{ij}(k,q)$. Furthermore, the dressing ratio D_r can be calculated using the array of dressing ratio calculation $DR_{ij}(k,q)$.

5.4. Some Results

As explained in Section 5.1-3, the grinding wheel surface after dressing can be realized by considering the real surface profile of a grinding wheel and the resultant sectional profile of multiple passes of dresser simultaneously. At first, the surface profile of the grinding wheel is simulated as shown in Fig. 5.12 (as illustrated in section 5.1).

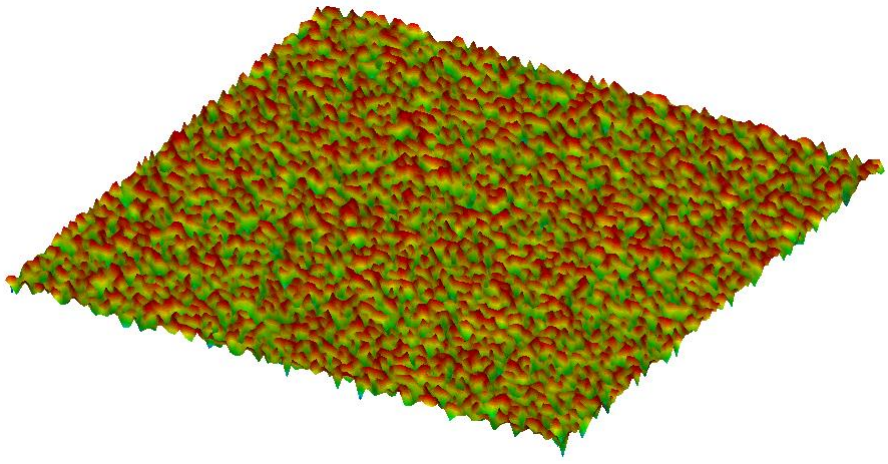

Figure 5.12. Simulated grinding wheel surface (scale: highest 0 μm, lowest -22 μm)

Afterwards, the resultant sectional profile of multiple passes of dresser is simulated as

presented in Fig. 5.2 (as illustrated in section 5.2) for the dressing conditions as listed in Table 5.2. Finally the 3D grinding wheel surface after dressing is generated as displayed in Fig. 5.3 in accordance with the strategy as described in section 5.3 for the dressing conditions as listed in Table 5.2.

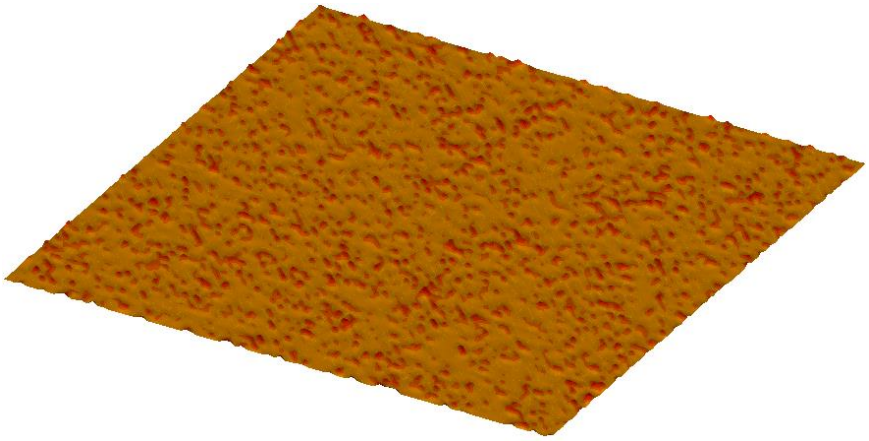

Figure 5.13. Simulated surface of the resultant sectional profile (scale: highest 0 μm, lowest -4 μm)

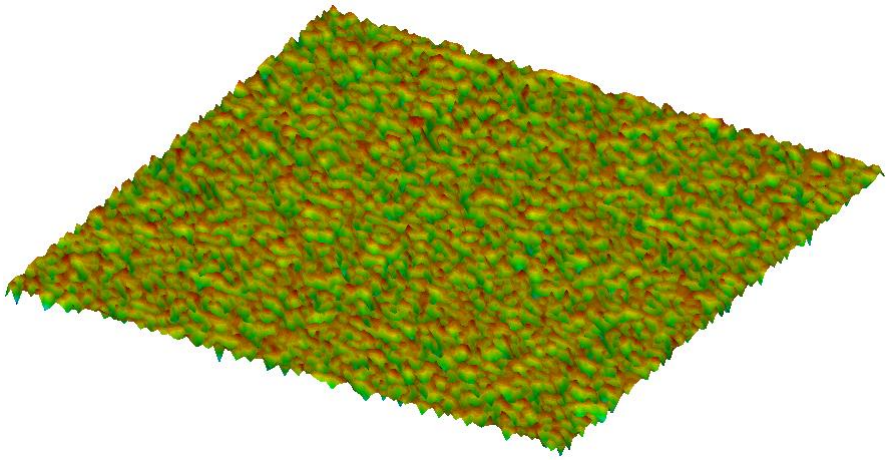

Figure 5.14. Grinding wheel surface after dressing (scale: highest 0 μm, lowest -25 μm)

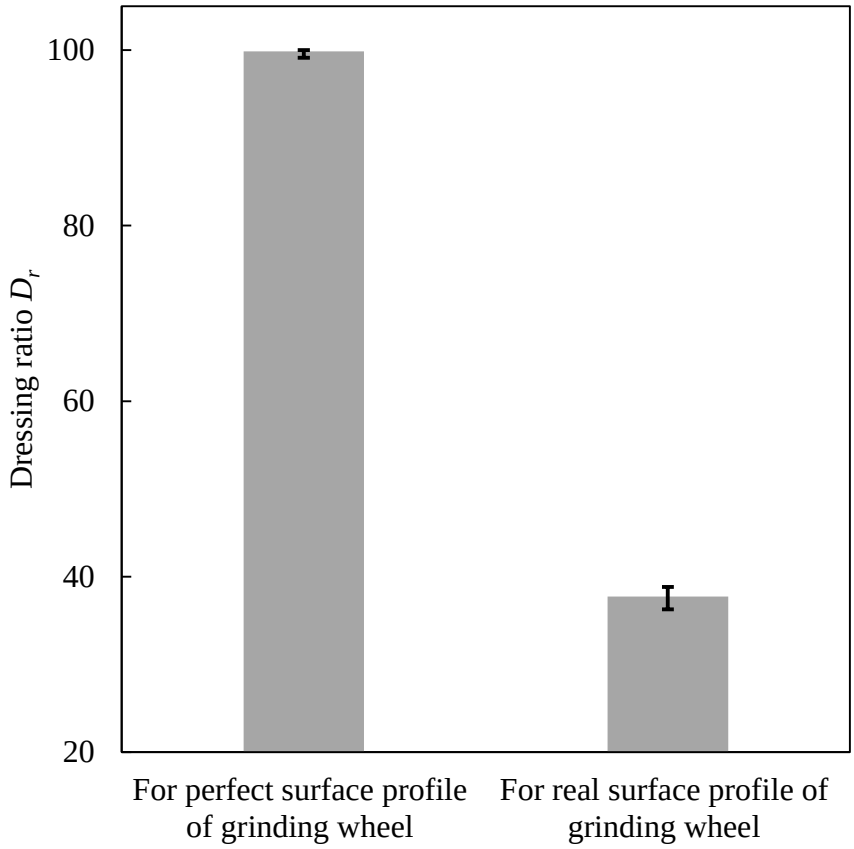

Figure 5.15. Comparison of dressing ratio for perfect and real surface profile of grinding wheel (for up-cut, VR = +0.7, t = 2 μm, N_D = 2 and f_d =1010 mm/min, No of Simulation = 100).

The dressing ratio for perfect surface profile of grinding wheel (z = 0) is higher than that of real surface profile of grinding wheel ($z \leq 0$) as the contact between the diamond grit of the RDD and the grinding wheel surface is larger in case of perfect surface profile of grinding wheel. Here, section 4.3 can be recalled where dressing ratio, D_r = 1 (100% dressing) is achieved (as shown in Fig. 4.5 and 5.15) after 2nd pass of dresser for up-cut, VR = 0.7, t = 2 μm and f_d =1010 mm/min. However, the dressing ratio is D_r = 0.38 (38%) for the same dressing conditions (as shown in Fig. 5.15) if the strategy illustrated

in section 5.1-3 is applied, i.e., the real surface profile of grinding wheel is considered. It is also noticeable that the variation is higher for dressing ratio in case of real surface profile of grinding wheel than that of perfect surface profile of grinding wheel. Note that simulation is run for 100 times.

Chapter 6

Discussion and Concluding Remarks

Rotary diamond dressers are one of the most widely used dressers for the dressing of vitrified grinding wheels. The grinding wheel surface topography after dressing is an indicator of the effectiveness of dressing operation and, thereby, the effectiveness of grinding as a whole. During rotary diamond dressing, the rotating dresser travels the revolving grinding wheel surface once or several times so that the dresser grits could hit all most all points on the working surface of the grinding wheel. But the same point should not be hit several times by the dressing grits. Therefore, development of a method and computer-aided simulation for generating the grinding wheel surface topography for single/multiple passes of rotary diamond dresser is important. Using the proposed method and simulation, one can determine the effectiveness of certain dressing conditions beforehand. In addition, the computer-aided simulation can be used for optimizing the design variables of a rotary diamond dresser.

In this study, a relatively comprehensive dressing mechanism is developed for the rotary diamond dresser based on kinematic analysis that defines the relationship between the dressing conditions and the dressing trajectories of diamond grits formed on the working surface of a grinding wheel. The developed mechanism can determine the trajectories of dresser on the working surface of the a grinding wheel after dressing operations multiple times wherein the depth of cut is increased

after each pass.

A computer-aided simulation is developed based on the kinematic mechanism to generate the working surface topography of the grinding wheel for a given set of dressing conditions, i.e., the velocity ratio of the rotary diamond dresser to the grinding wheel, up-cut or down-cut dressing, and single-pass or multipass dressing. The simulation is used to determine the 2D dressing performance, i.e., whether or not the diamond grits come in contact with the working surface of the grinding wheel considering the effect of dressing trajectory length only. Using the simulation process, the maximum feed speed of the rotary diamond dresser in single-pass dressing and the minimum number of passes in multipass dressing required to realize complete dressing are examined. The following remarks can be made on the findings of 2D dressing performance evaluation of rotary diamond dresser.

1. The length of the dressing trajectory increases with increasing circumferential length of the diamond grits and increasing depth of cut.

2. The length of the dressing trajectory in the case of down-cut dressing is shorter than that in the case of up-cut dressing for a given velocity ratio of rotary diamond dresser to the grinding wheel, and decreases with increasing in the velocity ratio, although an inflection point exists in the case of down-cut dressing.

3. The dressing conditions that realize complete dressing of the entire surface of the grinding wheel can be obtained from the dressing simulation, namely, the maximum feed speed of the dresser in single-pass dressing or the minimum number of passes in multipass dressing can be obtained.

4. In the case of down-cut dressing, it is almost impossible to achieve

complete dressing by tuning the feed speed of the dresser in single-pass dressing.

5. In multipass dressing, the minimum number of passes required to achieve the complete dressing is larger in the case of down-cut dressing than in the case of up-cut dressing.

In this study, three-dimensional topography of the grinding wheel surface after dressing is also generated, by considering real surface profile of grinding wheel ($z \leq 0$), which is used for 3D dressing performance analysis. The effectiveness of 3D simulation was demonstrated by examining the dressing ratio for the dressing conditions which realize complete dressing in case of 2D simulation. After the analysis, it is found that the dressing ratio of 3D simulation is less than half of 2D simulation for same dressing conditions. This is due to the fact that the contact between the diamond grit of rotary diamond dresser and the grinding wheel surface is smaller if real surface profile of grinding wheel is considered compared to perfect surface profile of grinding wheel ($z = 0$). It is also evident that the variation is higher for dressing ratio in case of real surface profile of grinding wheel than that of perfect surface profile of grinding wheel. The simulated topographies of the grinding wheel surface are expected to be used as a benchmark to understand the actual mechanism of dressing, in which cutting as well as the abrasion and fracture of abrasive grits and vitrified bonds occur.

In conclusion, a comprehensive dressing mechanism is developed to determine the general properties of the dressing trajectory on the grinding wheel surface for rotary diamond dressing. Afterward, computer-aided simulation is developed for the generation of two-dimensional and three-dimensional topography of grinding wheel surface after dressing. This method and computer-aided simulation

is an effective tool to comprehend the dressing mechanism and to predict the dressing performance. In addition, the study is concerted on the generation of grinding wheel surface topography after multiple passes of dresser, which has not been investigated beforehand. Finally, it could be stated that this research would definitely play a role in the development of abrasive technology, especially researchers and manufacturers of dressing and grinding tools.

Bibliography

[1] Malkin, S., *Grinding technology: Theory and applications of machining with abrasives*, (1989), Ellis Horwood Limited, pp.79-106.

[2] Rowe, W.B. *Principles of Modern Grinding Technology*, (2009), William Andrew Publishing, pp. 59-78.

[3] Jackson, M.J., Khangar, A., Chen, X., Robinson, G.M., Venkatesh, V.C., Dahotre, N.B., Laser cleaning and dressing of vitrified grinding wheels, *Journal of Materials Processing Technology*, Vol. 185,(2007), pp.17–23.

[4] Liao, W.T., Tang, F., Qu, J., Blau, P.J., Grinding wheel condition monitoring with boosted minimum distance classifiers, *Mechanical Systems and Signal Processing*, Vol. 22, No. 1(2008), pp. 217-232.

[5] Kure grinding wheel, 2013, http://en.kuretoishi.com/support/knowledge/bond.html (accessed on August 30, 2013).

[6] Wegener, K., Hoffmeister, H.-W., Karpuschewski, B., Kuster, F., Hahmann, W.-C. and Rabiey, M., Conditioning and monitoring of grinding wheels, *CIRP Annals-Manufacturing Technology*, Vol. 60, No. 2 (2011), pp. 757-777.

[7] Axinte, D.A., Stepanian, J.P., Kong, M.C. and McGourlay, Abrasive waterjet turning-An efficient method to profile and dress grinding wheels, *International Journal of Machine Tools and Manufacture*, Vol. 49, No. 3-4 (2009), pp. 351-356.

[8] Wang, X.Y., Kang, R.K, Xu, W.J., Wang, L.J., Guo, D.M., Laser dressing of resin-bond diamond grinding wheel, *Int. J. of Manufacturing Technology and Management*, Vol. 12, No.1/2/3 (2007), pp. 246-258.

[9] Hosokawa, A., Ueda, T., Yunoki, T., Laser Dressing of Metal Bonded Diamond Wheel, *CIRP Annals - Manufacturing Technology*, Vol. 55, No.1 (2006), pp. 329-332.

[10] Klink, A., Wire electro discharge trueing and dressing of fine grinding wheels, *CIRP Annals - Manufacturing Technology*, Vol. 59, No. 1 (2010), pp. 235-238.

[11] Xie, J., Tamaki, J., An experimental study on discharge mediums used for electro-contact discharge dressing of metal-bonded diamond grinding wheel, *Journal of Materials Processing Technology*, Vol. 208, No. 1-3, (2008), pp.

239-244.

[12] Kubo, A., Tamaki, J., Development of solid-type diamond rotary dresser utilizing CVD diamond disc application to low-speed dresser, *Key Engineering Materials*, Vol. 329 (2007), pp.187-194.

[13] Tawakoli, T., Daneshi, A., T-dress, A novel approach in dressing and structuring of grinding wheels, *Advanced Materials Research*, Vol. 565(2012), pp. 217-221.

[14] Mochida, M., Kubo, A., Tamaki, J., Harano, K., Sumiya, H. and Ullah, A.M.M.S., Performance of newly developed single-point diamond dresser in terms of cutting-point rake angle, *Advanced Materials Research*, Vol. 565 (2012), pp. 205-210.

[15] Huang, H., Effects of trueing/dressing intensity on trueing/dressing efficiency and grinding performance of vitrified diamond wheels, *Journal of Materials Processing Technology*, Vol. 117, No. 1-2 (2001), pp. 9-14.

[16] Yamauchi, K., Takagi, J., Ohzeki, H. and Ishigami, H., Study on internal grinding of small bore, *Journal of the Japan Society for Abrasive Technology*, Vol. 45, No.9 (2001), pp. 437-441. (In Japanese)

[17] Yokogawa, M. and Furukawa Y., Dressing Performance of Prismatic Monocrystalline Diamond Dresser, *Journal of the JSPE*, Vol.60, No. 6 (1994), pp.803-807. (In Japanese)

[18] Mochida, Y., Nishioka, T., Kubo, A., Tamaki, J., Evaluation of diamond dressers and estimation of grinding performance by dressing force measurement, *International Journal of Abrasive Technology*, Vol. 3, No.1 (2010), pp. 37-50.

[19] Kim, S. and Ahn, J.H., Decision of dressing interval and depth by the direct measurement of the grinding wheel surface, *Journal of Materials Processing Technology*, Vol. 88 (1999), pp. 190-194.

[20] Linke, B. and Klocke, F., Temperature and wear mechanisms in dressing of vitrified bonded grinding wheels, *Manufacture*, Vol. 50, No. 6 (2010), pp. 552-558.

[21] Doman, D.A., Warkentin, A., and Bauer, R., A survey of recent grinding wheel topography models, *International Journal of Machine Tools and Manufacture*, Vol. 46 (2006), pp. 343-352.

[22] Horng, T.L., A model to simulate surface roughness in the pad dressing process, *Journal of Manufacturing Science and Engineering*, Vol. 21 (2007), pp.1599-1604.

[23] Klocke, F. and Linke, B., Mechanisms in the generation of grinding wheel topography by dressing, *Production Engineering Research and Development*, Vol.

2 (2008), pp.157-163.

[24] Baseri, H., Razaei, S.M., Rahimi, A. and Saadat, M., Analysis of the disc dressing effects on grinding performance-Part 1: Simulation of the disc dressed wheel surface, *Machining Science and Technology*, Vol. 12 (2008), pp. 183-196.

[25] Bzymek, Z.M., Duzy, G.M. and Mindek, R.B.J., Virtual truing and dressing of grinding wheel, *Key Engineering Materials*, Vol. 389-390, (2009), pp. 362-367.

[26] Moritomo S, Ota M, Uchiyama K, Dressing of grinding wheel (part-1)-Dressed ratio and performance of grinding wheel, *The Proceedings of the Annual Meeting of the JSPE*, (1984), pp. 471-472. (In Japanese)

[27] Yokogawa, M., and Furukawa, Y., Development of a rotary diamond dresser for superabrasive grinding wheel, *The Proceedings of the Autumn Meeting of the JSPE*, (1990), pp.411-412. (In Japanese)

[28] Yokogawa, M., and Furukawa, Y., Dressing mechanism of rotary diamond dresser, *Proceedings of the JSPE Autumn Meeting*, (1991), Japan, pp.441. (In Japanese)

[29] Yokogawa, M., and Furukawa, Y., Dressing accuracy of superabrasive wheels dressed by kelly driven rotary diamond dresser, *JSPE Journal*, Vol. 55(12) (1989), pp.2254. (In Japanese)

[30] Chowdhury M.A.K., Tamaki J., Kubo A., and Ullah A.M.M.S., An analytical model of rotary diamond dressing, *The proceedings of the JSPE Annual meeting*, (September 3, 2011), Hakodate, Japan, pp. 105-106.

[31] Chowdhury M.A.K., Kubo A., Tamaki J. and Ullah S., Algorithms for simulating dressing process of rotary diamond dresser, *The proceedings of the JSPE Annual meeting*, (September 1, 2012), Muroran, Japan, pp. 11-12.

[32] Chowdhury M.A.K., Kubo A., Tamaki J., and Ullah A.M.M.S., Computer-aided simulation of rotary diamond dressing based on kinematic analysis, *Journal of Advanced Mechanical Design, Systems, and Manufacturing*, Vol. 7, No. 4 (2013), pp. 506-520.

[33] Kubo A., Chowdhury M.A.K., Tamaki J., and Ullah A.M.M.S., Visualization of grinding wheel surface generated by rotary diamond dresser, *The Proceedings of the Japan Society for Abrasive Technology Annual meeting*, ABTEC 2012, (September 1, 2012), Kyoto, Japan, pp. 24-27. (In Japanese)

[34] Kubo A., Chowdhury M.A.K., Tamaki J., and Ullah A.M.M.S., Visualization of 3D topography of grinding wheel surface dressed by rotary diamond dresser, *The Proceedings of the Japan Society for Abrasive Technology Annual meeting*,

ABTEC 2013, (August 28, 2013), Tokyo, Japan, pp. 275 -280. (In Japanese)

[35] Kubo A., Chowdhury M.A.K., Noda S, Tamaki J., and Ullah A.M.M.S., Visualization of 3D topography of grinding wheel surface dressed by rotary diamond dresser, *Advanced Materials Research*, Vol. 797 (2013), pp.751-756.

[36] Chowdhury M.A.K., Tamaki J., Kubo A., and Ullah A.M.M.S., Visualization of grinding wheel surface topography for multiple passes of rotary diamond dresser, *Advanced Materials Research*, Vol. 565 (2012), pp. 222-227.

[37] Yamaguchi T., Higuchi M., Shimada S., Matsumori N. and Ogura H., Fractal modeling method for 3D structure of vitrified-bonded wheel, *Precision Engineering*, Vol. 3, No. 1 (2007), pp. 40-46.

[38] Sharif Ullah A.M.M., Tamaki J., Kubo A., Modeling and Simulation of 3D Surface Finish of Grinding, *Advanced Materials Research*, Vol. 126-128 (2010), pp. 672-677.

Appendix
List of Figures and Tables

List of Research Achievements

[1] M.A.K. Chowdhury, A. Kubo, J. Tamaki, and A.M.M.S. Ullah. Computer-aided simulation of rotary diamond dressing based on kinematic analysis, *Journal of Advanced Mechanical Design, Systems, and Manufacturing*, Vol. 7, No. 4, Pages 506-520, 2013. [DOI: http://dx.doi.org/10.1299/jamdsm.7.506] [Publisher: JSME, Japan]

[2] A. Kubo, M.A.K. Chowdhury, S. Noda, J. Tamaki, and A.M.M.S. Ullah. Visualization of 3D topography of grinding wheel surface dressed by rotary diamond dresser, *Advanced Materials Research*, Vol. 797, Pages 751-756, 2013. [DOI: 10.4028/www.scientific.net/AMR.797.751] [Publisher: Trans Tech, Switzerland]

[3] M.A.K. Chowdhury, J. Tamaki, A. Kubo, and A.M.M.S. Ullah. Visualization of grinding wheel surface topography for multiple passes of rotary diamond dresser, *Advanced Materials Research*, Vol. 565, Pages 222-227, 2012. [DOI: 10.4028/www.scientific.net/AMR.565.222] [Publisher: Trans Tech, Switzerland]

[4] A. Kubo, M.A.K. Chowdhury, J. Tamaki, and A.M.M.S. Ullah. Visualization of grinding wheel surface generated by rotary diamond dresser, *The Proceedings of the Japan Society for Abrasive Technology Annual Meeting* (ABTEC 2013), Tokyo, Japan, August 28, 2013, Pages 275 -280. (In Japanese)

[5] M.A.K. Chowdhury, A. Kubo, J. Tamaki and S. Ullah. Algorithms for simulating dressing process of rotary diamond dresser, *The Proceedings of the Japan Society for Precision Engineering Annual Meeting*, Muroran, Japan, September 1, 2012, Pages 11-12.

[6] A. Kubo, M.A.K. Chowdhury, J. Tamaki, and A.M.M.S. Ullah. Visualization of grinding wheel surface generated by rotary diamond dresser. *The Proceedings of the Japan Society for Abrasive Technology Annual Meeting* (ABTEC 2012), Kyoto, Japan, August 29, 2012, Pages 24-27. (In Japanese)

[7] M.A.K. Chowdhury, J. Tamaki, A. Kubo, and A.M.M.S. Ullah. An analytical model of rotary diamond dressing, *The Proceedings of the Japan Society for Precision Engineering Annual Meeting*, Hakodate, Japan, September 3, Pages 105-106.

Acknowledgments

My first debt must go to my advisor, Professor Jun'ichi Tamaki, Department of Mechanical Engineering, Kitami Institute of Technology, Japan, for his vision encouragement, suggestions and support throughout this study.

I gratefully acknowledge the suggestions and comments that I received from my doctoral thesis examination committee members, Dr. Jun'ichi Tamaki, Dr. A.M.M. Sharif Ullah in the Department of Mechanical Engineering, Dr. Atsuro Sannami in the Department of Computer Science, Dr. Jun-ichi Shibano, Dr. Soichiro Suzuki in the Department of Mechanical Engineering, at Kitami Institute of Technology.

I express my sincere appreciations to Mr. Akihiko Kubo, Mr. Shoma Noda and others in the Micro-Nano Machining Laboratory at Kitami Institute of Technology for providing me with the invaluable assistance during the course of my doctoral study. My sincere appreciations also go to the International Center at Kitami Institute of Technology for supporting me in different ways.

I would not have envisaged this path if not for my parents, Mr. Chowdhury and Mrs. Jasmine, who instilled within me a love of creative pursuits and science. To my parents, thank you. My sisters, Naila and Roksana, have also been the best of friends along this journey. This thesis would not be possible without the love and constant support of my wife, Kumkum, and my daughter, Wajeeha. Finally, I dedicate this thesis to my parents and family, wife, Wajeeha and my beloved country. I love you all dearly.